Characterization of *Not* homeobox genes during development in *Nematostella vectensis*

By Astrid Medhus

This thesis is submitted in partial fulfilment of the requirements for the degree of Master of Science

Department of Biological Sciences

Faculty of Mathematics and Natural Sciences

University of Bergen

June 2021

Acknowledgments

The work presented in this thesis was performed at the Sars International Centre for Marine Molecular Biology, University of Bergen, from August 2020 to June 2021.

A lot of people contributed to this project and deserves to be thanked. First of all, I have to thank my main supervisor Fabian Rentzsch for allowing me to do this amazing project. Your office door was always open, and you inspired me with your genuine passion for science. Thank you for always having time for me, no matter how busy you were, especially in the last couple of months.

This would not have been possible without my co-supervisor James Gahan. Thank you for all your wisdom, your patients with me in the lab and for always having time to answer my many questions. I have learned so much from you, and I owe you a huge thank you for assisting me in the writing process. I am also very thankful for our friendship outside the lab.

I am grateful for the opportunity of being part of such a great lab. All the people of S8 made me feel so welcome. Henriette for being an encyclopedia on everything lab-related and always having time to help me out. Eileen for taking such good care of the animals, and always brightening our day with your positive energy. Alexis for always being the voice of reason and a good friend. Mark, Natascha and Linda for all the fun times and discussion in the lab, and Ivan, Oceane, Fatemeh and Quentin for making me feel so welcome. I also want to thank Marta for starting the preliminary work on the *NvNot* genes and generating a *NvNotE::GFP* transgenic reporter line. I also must thank the great people of Sars, it has been an amazing place to do my master. Thankful for all the new friendships, the social events (although restricted) and the great hikes!

Lastly, I must thank my family for the continuous support, especially my parents for putting up with me and keeping me company at the cabin during home office days. You made a tedious situation, very enjoyable. A special thank you to my boyfriend for supporting me and at least pretending to understand what I do.

Table of Contents

Selected abbreviations

Hpf	Hours post fertilization
Dpf	Days post fertilization
CNS	Central nervous system
BMP	Bone morphogenetic proteins
NPC	Neural progenitor cell
Sog	Short gastrulation
Dpp	Decapentaplegic
GMC	Ganglion mother cell
NEC	Neuroepithelial cells
RGC	Radial glia cells
IP	Intermediate progenitors
bHLH	Basic helix-loop-helix
ZMG	Zymogen gland cells
MGC	Mucous gland cells
Ilp	Preproinsulin-like peptide genes
Xnot	*Xenopus* notochord-specific
Flh	Floating head
NM	*Nematostella* medium
BSA	Bovine serum albumin
ISH	*In situ* hybridization
DFISH	Double fluorescence *in situ* hybridization
sgRNA	Single guide RNA
RT	Room temperature
O/N	Over night
HD	Homeobox domain

Abstract

The evolutionary origin of neurons and their relationship to other cell types is poorly understood. Neurons are a highly diverse cell type, with several cellular processes shared with gland/secretory cells. Similarities in the molecular machinery involved in vesicle trafficking in sensory neurons and secreting cells, supports a close evolutionary relationship of these cells. The cnidarian sea anemone *Nematostella vectensis* inhabits a phylogenetically informative position as part of the sister group to bilaterians, making it a suitable model organism to compare development of gland/secretory cells to the development of neurons. Gland/secretory cells in *Nematostella* were recently found to differentiate from *NvSoxB(2)*-expressing progenitor cells, which also give rise to neural cells. A microarray screen to reveal genes potentially functioning downstream of *NvSoxB(2),* identified the *Not* homeobox genes. In this study, we used *in situ* hybridization to establish a temporal and spatial expression pattern for *NvNotA*, *NvNotC* and *NvNotE*. *NvNotA* was found to be expressed in the mesendoderm, *NvNotC* in the aboral ectoderm and later in the mesendoderm, and *NvNotE* exclusively in the ectoderm. By double fluorescence *in situ* hybridization, *NvNotE* was found to be co-expressed with *NvMucin* throughout development, but not with a panel of genes expressed in neural cells. Furthermore, *NvNotE* was also found with fluorescence *in situ* hybridization and a transgenic reporter line to be expressed in *NvSoxB(2)*-expressing cells early in development, as well as in *NvInsm1*-expressing cells, which have previously been shown to give rise to both neural cells and gland/secretory cells. This study identifies the first transcription factor potentially involved in the development of a specific group of gland/secretory cells in *Nematostella*. We propose a cell differentiation trajectory in *Nematostella* where a post-mitotic group of *NvInsm1* expressing cells derived from a pool of *NvSoxB(2)*-expressing progenitors, gives rise to a group of *NvNotE*-expressing gland/secretory cells which also express *NvMucin*. Finally, CRISPR/Cas9 genome editing was successful in creating *NvNotE* mutant animals, which will allow further studies of both the function of *NvNotE* as well as the role of this population of gland/secretory cells in *Nematostella*.

1. Introduction

1.1 Evolutionary relationship between gland/secretory cells and neurons

The nervous system allows an organism to sense and react to its environment through chemical and/or electrical signals transmitted in a targeted and systematic manner (Schmidt-Rhaesa et al., 2015). The functional unit of the nervous system is the neuron, a highly specialized, but diverse cell type. Most neurons utilize action potentials and long processes known as neurites, to allow them to quickly conduct electrical signals, however, there are exceptions to this (Arendt, 2020; Kristan, 2016). The diversity of neuronal cell types makes them challenging to define (Burkhardt & Sprecher, 2017). In fact, "neuron-specific" features are specializations of basic cellular processes, like the molecular machinery involved in docking and secretion of vesicles (Arendt, 2020; Kristan, 2016). Many of what are considered typical neuronal features were already present before the evolution of the nervous system, an example being voltage-gated potassium channels in bacteria; another being the secretion machinery in choanoflagellates (Burkhardt & Sprecher, 2017; Burkhardt et al., 2011). Furthermore, Placozoa have no recognizable nervous system but do possess voltage-gated channels and structures that resemble synapses (Kristan, 2016). Gland cells around these synapse-like structures are found to express proteins found in bilaterian synaptic complexes like SNAP-25, complexin and synapsin in addition to the neuropeptide FMRFamide (Burkhardt & Sprecher, 2017; Hartenstein et al., 2017; Smith et al., 2014). This supports a model where an early secreting cell might have served as an evolutionary precursor of neurons as these conserved phenotypes, shared between secretory and neural cells, can be found in animals seemingly missing a nervous system (Brunet & Arendt, 2016; Jékely, 2021; Moroz, 2009).

As it appears that typical "neuronal" features are shared across species with and without a nervous system, these cellular mechanisms have been adopted to different functions during evolution. Comparing genomes, transcriptomic data and cell differentiation in different species will be beneficial in trying to unravel the origin of the nervous system and how it relates to other cell types.

1.2 Cnidarians

Historically, the use of model organisms has been limited to established organisms selected for their ease of culture and/or short generation time (e.g. *Drosophila melanogaster* and *Caenorhabditis elegans*) (Hedges, 2002). In recent years, a shift of focus has occurred, complemented by the availability of whole genome sequences, to model organisms that are of interest for their phylogenetic position or aspects of biology inherently interesting in the organism (Russell et al., 2017). As the sister group to bilaterians, cnidarians possess a phylogenetically informative position for understanding the evolutionary origin of a variety of different developmental processes (Figure 1.1 A) (Hejnol et al., 2009; Rentzsch et al., 2017).

The cnidarian phylum (jellyfish, hydroids, corals, and sea anemones) consists of approximately 10,000 species of mainly marine, invertebrate animals (Darling et al., 2005; Finnerty, 2001; Technau & Steele, 2012). Cnidarians are grouped into two main clades, Anthozoa and Medusozoa, broadly defined by the presence of a sessile polyp common to both with the addition of a free-swimming medusa in the medusozoans (Technau & Steele, 2012). In contrast to bilaterians, cnidarians are diploblastic (having two germ layers) along with a radial symmetry, although some anthozoans have an internal bilaterality (Technau & Steele, 2012).

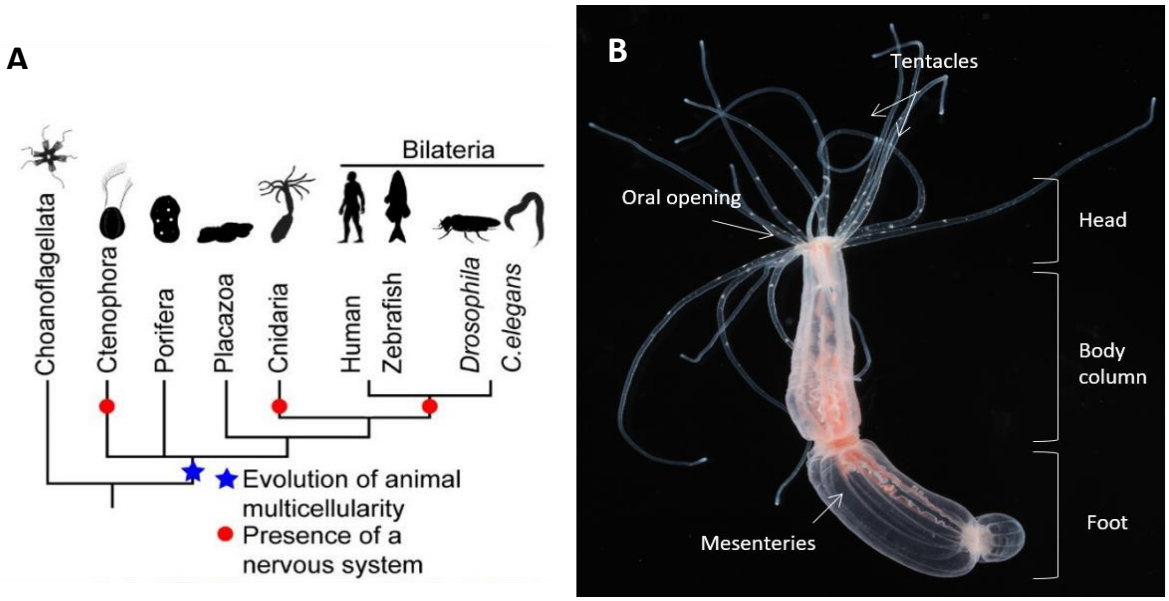

Figure 1.1: Phylogenetic tree showing cnidarians as sister group to bilaterians and adult *Nematostella vectensis.* **(A)** Simplified phylogeny showing Cnidaria as the sister group to Bilateria. Red circle indicates the presence of a nervous system and the evolution of animal multicellularity is indicated by blue star. Figure from (Gahan et al., 2020) (**B)** Adult *Nematostella* polyp with anatomical features indicated. Picture from Chiara Sinigaglia, Fabian Rentzsch lab.

There are several well-established cnidarian model organisms, like the anthozoan *Acropora millepora* giving key insight into issues like coral bleaching (Fuller et al., 2020; Technau & Steele, 2012), and perhaps the most well-known, the hydrozoan *Hydra,* one of the first model organism used for experimental developmental biology (Lenhoff & Lenhoff, 1989; Trembley, 1744). However, the anthozoan *Nematostella vectensis* was the first cnidarian to have its genome sequenced and has quickly become one of the preferred cnidarian model organisms (Putnam et al., 2007).

1.2.1 Nematostella vectensis

Hand and Uhlinger established a protocol in 1992 enabling *Nematostella* to be kept in culture throughout its life cycle (Hand & Uhlinger, 1992). This sea anemone has since been a preferred cnidarian model organism due to its relatively short generation time of about 4 months, inducible spawning throughout the year, and its ease of genetic manipulation (Darling et al., 2005; Layden et al., 2016; Technau & Steele, 2012). *Nematostella* is a burrowing sea anemone that can be found in brackish waters on the Pacific coast of North America as well as on the east and west coast of the North Atlantic (Darling et al., 2005). In the wild, the adult polyp rarely exceeds 2 cm (Williams, 1979), however, in laboratory conditions, its average length is around 10 cm due to the abundance of food. The body structure resembles a hollow tube with one opening functioning as both the mouth and anus. The oral opening is surrounded by a ring of 16 tentacles used for capturing prey (Williams, 1975). The aboral part of the body column, the foot, is typically buried in the substrate when found in nature (Figure 1.1 B) (Williams, 1975). In 2007 the whole genome sequence of *Nematostella* was made available (Putnam et al., 2007), enabling genome editing tools to be adapted such as CRISPR/Cas9 to be adapted (Ikmi et al., 2014), as well as other well-established methods like short-hairpin RNA (He et al., 2018; Karabulut et al., 2019) morpholino gene knockdown (Layden et al., 2013), and the generation of stable transgenic lines (Renfer et al., 2010). Altogether, these techniques this make *Nematostella* an increasingly popular model organism in evolutionary developmental biology (Layden et al., 2016).

Nematostella is a dioecious species which releases its gametes for external fertilization (Figure 1.2 A) (Fritzenwanker & Technau, 2002). The gametes are formed in the mesenteries and, when mature, the eggs are squeezed through the endodermal epithelial and into the gastric cavity

before it is released as a package of eggs with a gelatinous wrapping (Fritzenwanker et al., 2007). The males release free-swimming sperm. The unfertilized egg has an animal-vegetal polarity indicated by the female pronucleus located at the animal pole (Fritzenwanker et al., 2007; Lee et al., 2007). The first cleavage starts at the future oral pole. At the very beginning, the blastomeres are not fully separated as cytokinesis occurs earliest at the 4-cell stage. At the 8-cell stage, the blastomeres are fully separated. Between the 16- and 32-cell stage, the epithelium starts to form. At the 64-cell stage a cycle of invagination and evagination starts as the cells become polarized with their nuclei moving closer to the apical surface (Fritzenwanker et al., 2007). At around 20 hours post fertilization (hpf) the epithelium starts to invaginate as gastrulation initiates at the animal pole (Figure 1.2 B). The blastopore originates from the animal pole and the oral-aboral axis corresponds to the animal-vegetal axis (Fritzenwanker et al., 2007; Lee et al., 2007). Along with the mesendoderm, a part of the ectoderm internalizes to form the ectodermal component of the pharynx (Figure 1.2 C) (Fritzenwanker et al., 2007; Steinmetz et al., 2017). At 48-72hpf a free-swimming larva emerges from the egg package, and a ciliated organ on the aboral end, the apical tuft, is generated (Figure 1.2 D). The animal gradually elongates, and eventually settles and loses its apical tuft (Fritzenwanker et al., 2007). At around 7 days post fertilization (dpf), four tentacle buds are formed around the oral opening marking the shift to a primary polyp (Figure 1.2 E). As the animal develops, more tentacles are formed to facilitate feeding behavior (Fritz et al., 2013; Ikmi et al., 2020).

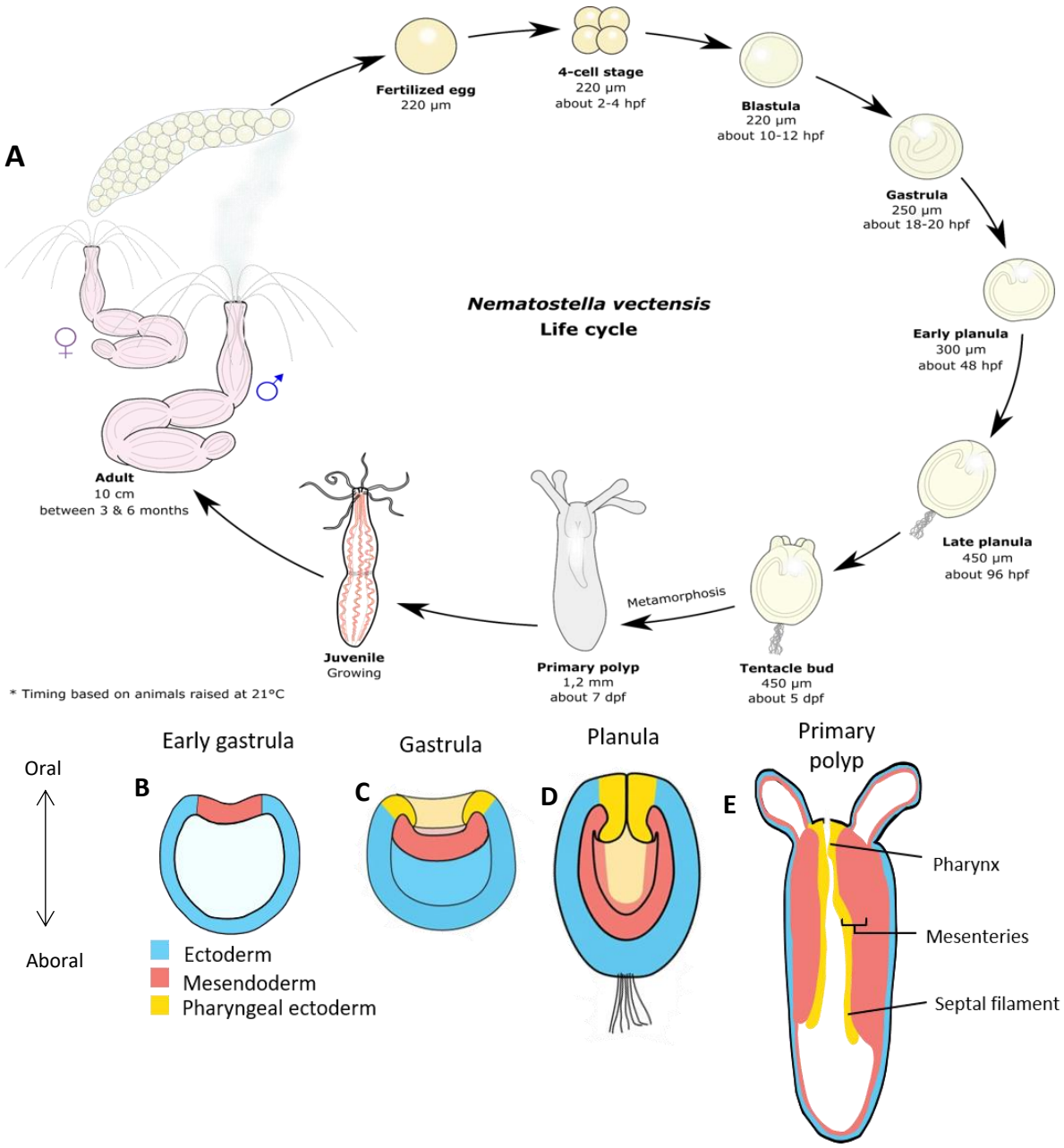

Figure 1.2: *Nematostella vectensis* sexual life cycle and development. (A) Gametes are released for external fertilization and at 2-4hpf the egg starts to divide. Gastrula starts at about 20hpf and at approx. 5dpf tentacle buds are formed and the animal settles and undergoes metamorphosis to a primary polyp at around 7dpf. In about 3-6 months the animal reaches sexual maturity. Schematics by Quentin I. B. Lemaître, 2021. **(B)** Development of *Nematostellla* embryo from early gastrula to primary polyp with germ layers indicated. Figure modified from (Steinmetz et al., 2017).

As a diploblastic organism, *Nematostella* has two germ layers: ectoderm, and a germ layer thought to be homologous to both the bilaterian endoderm and mesoderm called the mesendoderm (Figure 1.2 B) (Technau & Steele, 2012). The two germ layers are separated by the extracellular matrix, the mesoglea (Martindale et al., 2004). The pharynx extends down into the gastric cavity continuing into the folds of the gastrodermis, the mesenteries (Figure 1.2 B, Figure 1.3) (Burton & Finnerty, 2009; Martindale et al., 2004; Renfer et al., 2010). *Nematostella* has a primary oral-aboral axis running along the length of the body column, with a directive axis oriented orthogonally to the primary axis (Rentzsch & Technau, 2016; Technau & Steele, 2012). Eight mesenteries extend along the oral-aboral axis, arranged radially with two primary mesenteries forming first (Layden et al., 2016). The orientation of the retractor muscles on the mesenteries (Figure 1.3 C), along with a ciliated groove on one side of the pharynx, gives a bilateral symmetry found in most anthozoans in contrast to the radial symmetry along the oral-aboral axis found in medusozoans (Figure 1.3) (Technau & Steele, 2012).

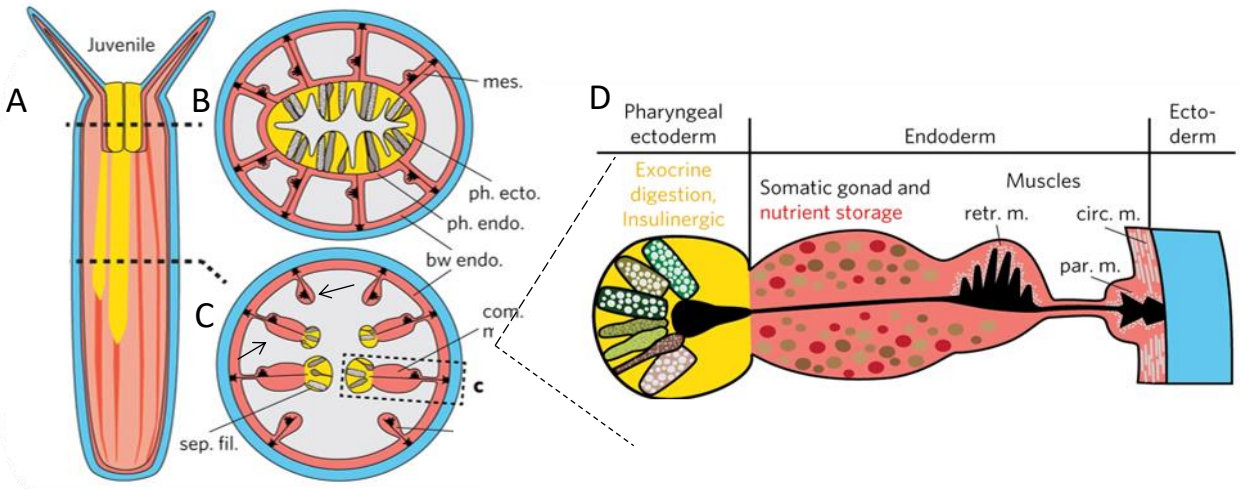

Figure 1.3: Schematic cross-section of juvenile mesenteries. (A-C) Cross section of a polyp shown along the oral-aboral axis (sep. fil; septal filament, bw endo.; body wall endoderm, ph ecto/endo; pharyngeal ectoderm/endoderm, mes.; mesenteries). (C) Arrows indicate opposite orientation of retractor muscles on the mesenteries. **(D)** Cross section of a mesentery**.** The mesendodermal part of the mesenteries consists of three types of muscle (retr.; retractor, par.; parietal, circ.; circular) and either somatic gonads or nutrient storage tissue. The most distal part consists of the septal filament composed of the pharyngeal ectoderm containing cnidocytes and gland/secretory cells involved in digestion and uptake of nutrients. Figure modified from (Steinmetz et al., 2017)

The mesendodermal part of the mesenteries, closest to the body wall, contains the retractor and parietal muscle, followed by either a nutrient storing trophic tract or a somatic gonad that produce gametes depending on its position along the oral-aboral axis (Figure 1.3) (Babonis et al., 2019; Steinmetz et al., 2017). The septal filament is the most distal part and is derived from the pharyngeal ectoderm. The septal filament possesses both cnidocytes (stinging cells) and an array of gland/secretory cells involved in digestion and uptake of nutrients (Steinmetz, 2019).

1.3 Development of neurons and gland/secretory cells in bilaterians

1.3.1 Development of neurons in bilaterians

In bilaterians, nervous system development typically starts with the specification of the neuroectoderm, the area of the ectoderm that has the competence to generate neurons. The neurons are produced through a series of asymmetric and symmetric cell divisions of neural stem cells, giving rise to various types of neural progenitor cells (NPC) and subsequently differentiating neurons (Hardwick et al., 2015; Taverna et al., 2014). Symmetric divisions give rise to identical cells, for example to expand a population of progenitor cells or to generate two differentiating neurons of the same type. Asymmetric divisions produce two cells with different developmental potential, for example one progenitor cell and one neuron or two different types of neurons (Florio & Huttner, 2014; Hardwick et al., 2015).

Neural progenitor cells of *Drosophila melanogaster,* neuroblasts, originate from the neurogenic ectoderm which consist of the ventral neuroectoderm and the procephalic neuroectoderm (Campos-Ortega, 1995). The ventral ectoderm will give rise to the ventral nerve cord and the subesophageal ganglion, while the procephalic neuroectoderm gives rise to the brain hemispheres (Truman & Bate, 1988). As neurogenesis progresses, neuroblasts repeatedly undergo self-renewing asymmetric divisions (Zhong & Chia, 2008). To ensure two daughter cells with different potential, the cells get polarized along the apicobasal axis prior to division. The polarity is defined by the Par protein complex and a protein cassette related to heterotrimeric G protein signaling, linked together by Inscuteable (Insc) (Hartenstein & Wodarz, 2013). The Par proteins are already localized apically, and as the embryonic neuroblast starts to delaminate both the Insc and G-protein complex is recruited to the apical cortex. The Par protein redirects cell

fate determinants to the basal cortex creating a cell polarity. The G-protein cassette helps orient the mitotic spindle to its appropriate position (Hartenstein & Wodarz, 2013; Zhong & Chia, 2008). The subsequent cell division gives rise to a larger cell that retains the neuroblast identity, and a smaller cell exclusively containing the cell-fate determinants creating a ganglion mother cell (GMC), which will terminally divide into two post-mitotic neuronal/glial cells (Zhong & Chia, 2008).

Development of the vertebrate central nervous system (CNS), best studied in the mouse cortex, progresses through two major phases. First, a proliferation phase to expand the pool of NPCs and second, a phase of cell differentiation to generate the array of functional neurons and glial cells. Cell differentiation occurs from a pool of three neural progenitors, the neuroepithelial cells (NEC), radial glial cells (RGC) and intermediate (or basal) progenitors (IP) (Figure 1.4) (Florio & Huttner, 2014; Götz & Huttner, 2005; Hardwick et al., 2015). NECs expand the pool of progenitors by undergoing symmetric cell divisions during early development. As the cell goes through the cell cycle, the nucleus moves towards the ventricular surface (apical side) where it undergoes mitosis before moving back towards the basal position. This is known as interkinetic nuclear migration. Each of the daughter cells retains a portion of the apical membrane and basal processes (Götz & Huttner, 2005; Hardwick et al., 2015). Eventually NECs will start to undergo a transition to another type of progenitor cells, RGCs. The morphology of the cells elongates as they lose tight junctions and start to express glial specific genes. RGCs also demonstrate interkinetic nuclear migration, and they start to undergo proliferative asymmetric division. As the cell divides the daughter cell that inherits the basal process will remain as a progenitor cell. The other daughter cell is committed to the neuronal lineage, either through direct or indirect neurogenesis, creating intermediate progenitors (Götz & Huttner, 2005; Hardwick et al., 2015). The intermediate progenitors represent a more fate-restricted pool of NPCs. They vary in their processes and have different development potentials; however, they all lack contact with the ventricular surface (Götz & Huttner, 2005; Hardwick et al., 2015).

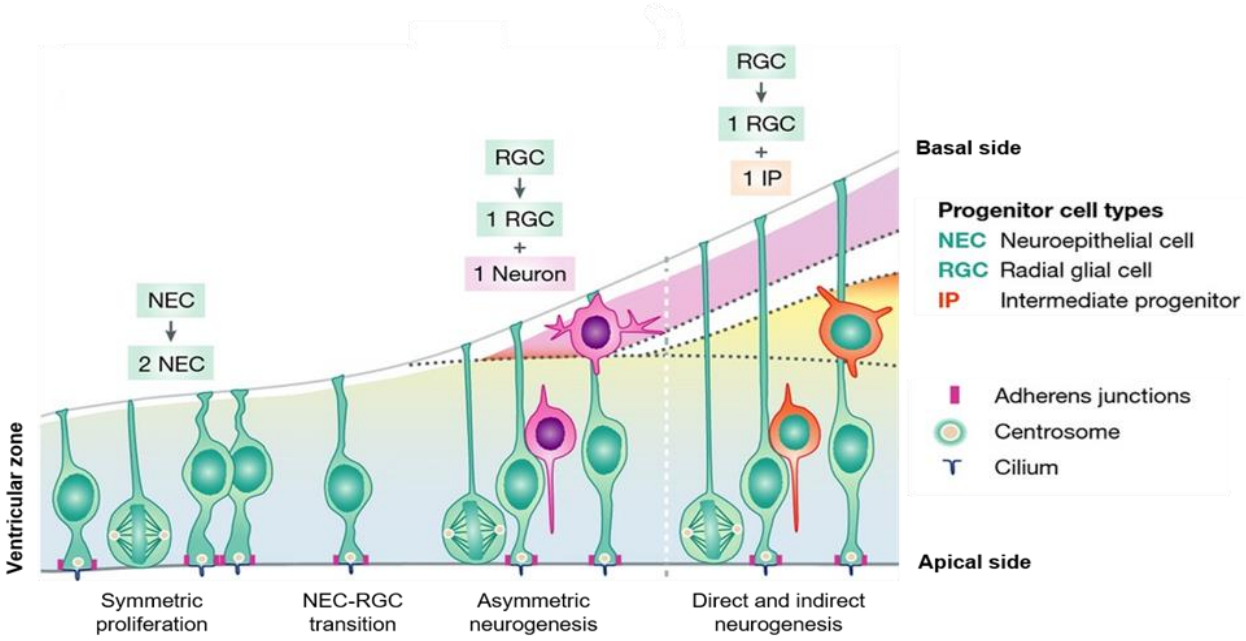

Figure 2.4: Development of the vertebrate central nervous system represented in the mouse cortex. Cell differentiation occurs from three different neural progenitors. Symmetric cell division of neuroepithelial cells (NEC) expands the pool of progenitors early in development. Later NEC transitions to Radial glial cell (RGC), which undergoes asymmetric division that either generate neuronal cells through direct neurogenesis or by indirect neurogenesis generating an intermediate progenitor (IP). Figure modified from (Florio & Huttner, 2014)

1.3.2 Development of gland/secretory cells in bilaterians

Gland/secretory cells produce and release substances (e.g hormones or mucous) either without the use of a duct (endocrine) or to an epithelial surface trough a duct (exocrine) (Freeman et al., 2020). Entero-endocrine cells are specialized secreting epithelial cells located, together with secretory gland cells, in the intestine of bilaterians (Hartenstein et al., 2017). Their cell body is positioned basally with a neck reaching towards the luminal surface of the epithelium. Basal processes (neuropods) interact with neural and non-neural cells of the gastrointestinal tract. Entero-endocrine cells use two structurally defined types of vesicles for secretion into the interstitial space through the basal cell membrane (Hartenstein et al., 2017). The electron dense interior of the dense core vesicles stores and releases peptides, while the smaller microvesicles resemble the ones found at synapses, containing neurotransmitters (Hartenstein et al., 2017). In fact, endocrine cells and sensory neurons have several functional, structural, and developmental properties in common. They express many of the same (or related) apical membrane receptors, which are involved in similar cellular mechanisms related to stimulus processing and docking, and

trafficking of vesicles. Proneural basic helix-loop-helix (bHLH) genes act in the differentiation of progenitor cells to secretory/gland cells, and later to entero-endocrine cells (Hartenstein et al., 2017). In addition, at least 15 peptides have been found in entero-endocrine cells in the mammalian gut, where the suggested homologs have been found to be expressed in neurons in *Drosophila* (Hartenstein et al., 2017). These similarities support a suggested evolutionary relationship between secretory and neuronal cells.

1.4 Development of neurons and gland/secretory cells in cnidarians

1.4.1 Development of neurons in cnidarians

Cnidarians are one of the earliest branching animal groups that possess a nervous system (Arendt et al., 2019). It is organized as a nerve net without brain-like centralization, though with regional differences (Kelava et al., 2015; Rentzsch et al., 2017). It consists of three main morphological classes of cells: sensory cells, ganglion cells (believed to act similarly to interneurons) and the phylum-specific cnidocytes (Richards & Rentzsch, 2015). Cnidocytes are stinging cells containing a collagenous capsule, the cnidocyst, which contains a harpoon-like thread used to inject venom (Wolenski et al., 2013). They are used in capturing of prey and for defense and are typically found in the epidermis and in tentacle tips (Babonis & Martindale, 2017; Wolenski et al., 2013). Sensory cells are elongated and make contact with the apical surface as well as the basal membrane, while ganglion cells are located near the basal part of the epithelium. Both sensory cells and cnidocytes have an apical sensory cilium. Common for all are the presence of neurites emerging from the basal side, creating a nerve net located both in the ectoderm and mesendoderm (Marlow et al., 2009; Nakanishi et al., 2012; Rentzsch et al., 2017).

The developmental origin of neurons in cnidarians is not uniform. Hydrozoans, including *Hydra,* contain a population of non-epithelial interstitial stem cells called i-cells (Bode et al., 1987; Denker et al., 2008; Gahan et al., 2016; Galliot et al., 2009). This is a population of self-renewing multipotent stem cells and acts as the source for neural cells as well as other cell types (Bursztajn & Davis, 1974). I-cells have only been identified in hydrozoans. However, a population of epithelial *NvSoxB(2)*-expressing progenitor cells has been identified in *Nematostella* (Figure 1.5) (Richards & Rentzsch, 2014). *NvSoxB(2)*$^{+}$ progenitor cells are first detectable throughout the

epithelium at blastula stage (Magie et al., 2005). Differentiation of neural cells starts around the gastrula stage in the ectoderm, concomitant with the appearance of NPC in the mesendoderm, which will give rise to the mesendodermal nervous system beginning at early planula stage (Nakanishi et al., 2012; Richards & Rentzsch, 2014). This neurogenic potential in both germ layers sets it apart from most bilaterians (Kelava et al., 2015). By polyp stage the nerve net is established with tracts of mesendodermal neurites running parallel to the mesenteries in addition to areas with higher density of neurons in the oral and pharyngeal regions (Watanabe et al., 2014). At this stage, cnidocytes can be found all over the ectoderm, including the pharynx and septal filaments, with higher densities in the tentacles (Babonis & Martindale, 2014; Zenkert et al., 2011)

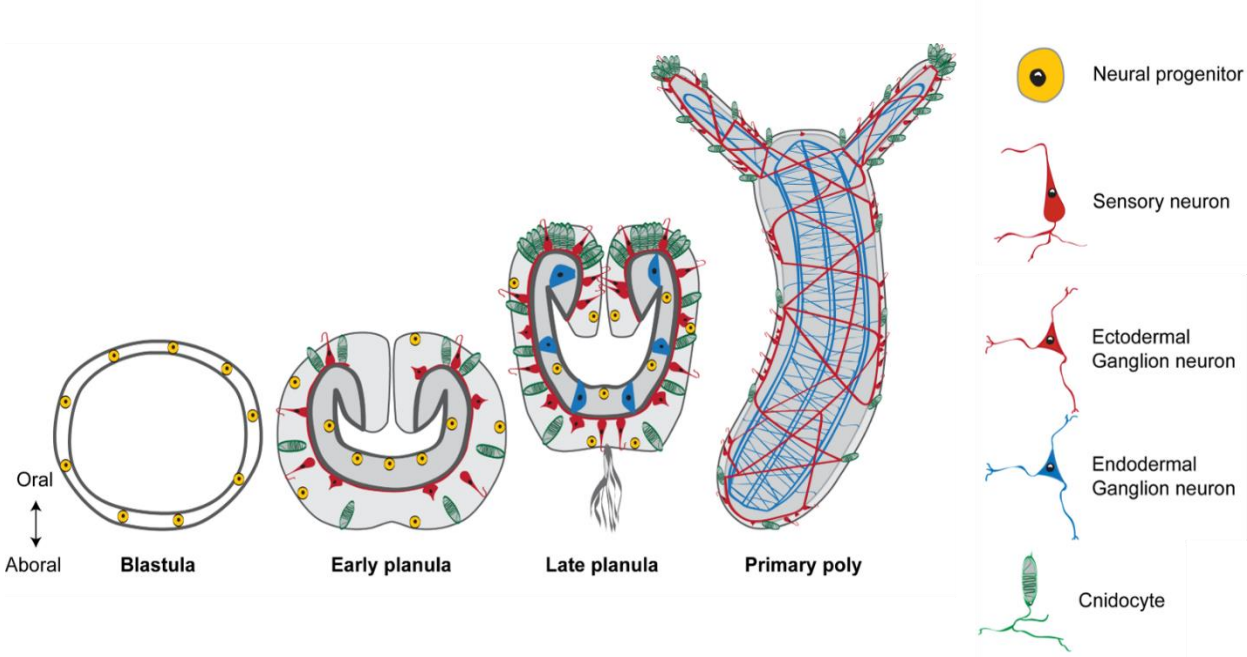

Figure 1.5: Neurogenesis in *Nematostella vectensis*. Neural progenitor cells in the mesendoderm and ectoderm give rise to sensory and ganglion neurons as well as cnidocyte during embryogenesis. At polyp stage neurons are connected in a nerve net in both the mesendoderm and ectoderm. Figure adapted by Océane Tournière from (Richards & Rentzsch, 2014)

Proneural bHLH genes have been identified in *Nematostella* and have been shown to act early in neurogenesis. *NvAshA*, a homolog of the achaete-scute family, is expressed in some *NvSoxB(2)*$^{+}$ cells early in neurogenesis, however only in non-proliferating cells suggesting a role in early differentiation (Richards & Rentzsch, 2015). Knockdown of *NvAshA* has been shown to lead to a loss of neural cells (Layden et al., 2012), while knockdown of another bHLH gene, *NvAth-like*

(atonal-like), results in a decrease in *NvAshA* expression. Unlike *NvAshA*, *NvAth-like* is co-expressed with *NvSoxB(2)*$^{+}$ in proliferating cells (Layden et al., 2012; Richards & Rentzsch, 2015). However, whether *NvAth-like* functions to initiate neurogenesis or to regulate the fate of pre-existing NPCs, remains elusive.

Finally, the Notch signaling pathway also functions in *Nematostella*. Notch signaling has been found to negatively regulate neurogenesis in *Nematostella*. Treatment with the γ-secretase inhibitor DAPT leads to inhibition of Notch signaling and subsequently an upregulation of *NvAshA* and *NvAth-like* expression and consequently an increase in neurogenic gene expression (Layden & Martindale, 2014; Marlow et al., 2012; Richards & Rentzsch, 2015). In addition, an increase of *NvSoxB(2)*$^{+}$ cells is also observed, suggesting that Notch signaling is required to limit the formation of progenitor cells.

Notwithstanding the apparent simplicity of the nervous system, its molecular regulation is more intricate than one might assume and shares several similarities with bilaterians (Darling et al., 2005; Technau & Steele, 2012). The progenitor cell marker, the HMG-box sox family transcription factor *NvSoxB(2)*, is related to the bilaterian SoxB1 and SoxB2 family of transcription factors expressed in developing neurons (Graham et al., 2003; Zhao & Skeath, 2002). In addition, similarly to their role in *Nematostella*, in bilaterians, bHLH transcription factors of both the atonal and achaete-scute families are critical for initiation of neurogenesis as well as neuronal-subtype specification (Bertrand et al., 2002). However, in most bilaterians *Ash* genes acts primarily in early proliferative neural progenitors contrasting with the described role of *NvAshA* in *Nematostella*. The Notch signaling pathway is also a known bilaterian neurogenesis regulator. As it acts in a similar manner in cnidarians, it shows a conserved role of Notch signaling.

1.4.2 Development of gland/secretory cells in cnidarians

The i-cells in *Hydra* give rise to non-neural cells like gametes and gland cells (Bode, 1996; Bode et al., 1987; Bursztajn & Davis, 1974). The gland progenitor cells are present in the ectoderm and subsequently migrate to the endoderm giving rise to two classes of gland cell, the zymogen gland cells (ZMG) residing in the gastric region and mucous gland cells (MGC) in the head. The MGC are comprised of granular MGCs and squamous MGCs (David, 2012; Siebert et al., 2008). Siebert et

al., recently constructed stem cell differentiation trajectories based on *Hydras* single-cell transcriptomes (Siebert et al., 2019). They discovered that neural and gland cell progenitors co-localized in several independent clustering analyses, leading them to suggest a model in which multipotent interstitial stem cells first differentiate into either a cnidocyte progenitor, or a bipotential gland/neuron progenitor in the ectoderm that will subsequently cross the extracellular matrix providing the endodermal layer with both gland and neural cells (Siebert et al., 2019).

Similarly to the i-cells in *Hydra*, the *NvSoxB(2)*-expressing progenitor cells in *Nematostella* contain proliferating cells able to generate all cnidarian neural classes, as well as also gland/secretory cells as shown by a transgenic line with expression of mOrange driven by the *NvSoxB(2)* promoter (Richards & Rentzsch, 2014; Tournière et al., 2021). However, in contrast to *Hydra* where gland cells are predominantly found in the endoderm (Gahan et al., 2016), gland/secretory cells in *Nematostella* have been observed in the tissue with ectodermal origin like the pharynx, the septal filaments, and the ectoderm of the body column (Babonis et al., 2019; Steinmetz et al., 2017). The pharynx has been shown to express transcription factors reminiscent of the transcription factor profile found for the endoderm of the bilaterian midgut and vertebrate pancreas, as well as containing exocrine and insulinergic cell-types (Steinmetz et al., 2017). These cells show expression of trypsinogen proteases, chitinases and triacylglyceride hydrolysing pancreatic lipase which suggest high protease activity. In addition, preproinsulin-like peptide genes (Ilp) are found to be expressed in the gland/secretory cells of the pharynx and septal filament. The only gland/secretory cells that are detected also in the mesendodermal tissue are the mucin-expressing mucous cell that are found in both germ layers (Steinmetz et al., 2017).

The ectodermal pharynx contains both zymogen- secreting (electron dense) and mucus-secreting (electron lucent) cells, however only the former can be found in the septal filaments (Babonis et al., 2019). The septal filament ends in either a unilobed or trilobed structure containing the exocrine tissue. The cell composition resembles that of the pharynx with cnidocytes and zymogen cells (Babonis et al., 2019; Steinmetz, 2019). A section of the mesenteries near the pharynx (oral opening), is rich in zymogen gland cells with secretory vesicles containing a heterogenous

content. The septal filaments in the aboral region, also contains zymogen gland cells, some with a motile apical cilium (Babonis et al., 2019).

1.5 Not homeobox genes

Homeobox genes encode transcription factors that regulate development and specification of cells through regulation of other genes (Holland, 2013). They all share a conserved approx. 60 amino acid sequence, called the homeobox, that folds into a helix-loop-helix-turn-helix structure. (Bürglin, 2013). The vast majority of homeobox transcription factors act during development, being required from early embryogenesis to late cell differentiation (Bürglin, 2013). Homeobox genes have been found in all metazoans (Mark et al., 1997; Negre & Ruiz, 2007).

In 1993, von Dassow et al. identified a novel homeobox gene in *Xenopus laevis* involved in regulating the formation of the notochord, now known as *Xnot* (*Xenopus* notochord-specific) (von Dassow et al., 1993). *Xnot* was first found to be expressed in the organizer region during gastrulation, and later identified as the earliest specific marker for the forming notochord. At the end of gastrulation, *Xnot* expression is restricted to cells determined to form the notochord and the floor plate of the neural tube (Gont et al., 1996; von Dassow et al., 1993; Yasuo & Lemaire, 2001).

The homolog of *Xnot* in zebrafish, *floating head* (*flh*), also plays a vital role in notochord development, primarily by repressing muscle fate (Yasuo & Lemaire, 2001). *Flh* mutant embryos lack the notochord altogether and develop somatic muscle in its place. It is believed that this happens from either of two scenarios: an incorrect specification of the notochord domain, or a respecification of the presumptive notochord to form muscle fibers. As for *Xnot*, *flh* is the earliest specific marker of the notochord, being essential for early gastrula cells developing correctly on an axial mesodermal pathway (Halpern et al., 1995; Talbot et al., 1995).

The chick homolog, *Cnot*, also harbors key features common with *Xnot*. *Cnot* expression is involved in specifying cells in the node, the equivalent to the organizer in Xenopus, and the notochord and neural plate (Stein & Kessel, 1995). Similarly, the mouse homolog of *Xnot*, *Noto*, is expressed in the organizer node in the forming notochord. However, *Noto* is also essential for ciliogenesis in the posterior notochord, and hence the left-right asymmetry of the body plan

(Beckers et al., 2007). In the Brachiopod *Terebratalia transversa,* the *TtrNot* is found to be expressed in a ring-like expression in the ciliated region of the apical lobe also suggesting a role in ciliogenesis (Altenburger et al., 2011).

Together it appears that Not homologs have a role in gastrulation, including germ layer and nervous system patterning. In chordates, Not genes are involved in notochord formation including left right patterning. In invertebrates, like cnidarians, the role of the Not homeobox genes remains unknown (Altenburger et al., 2011; Beckers et al., 2007; Gont et al., 1996; Halpern et al., 1995; Stein & Kessel, 1995; Talbot et al., 1995; von Dassow et al., 1993; Yasuo & Lemaire, 2001). The presence of Not homeobox genes in cnidarians establishes its existence prior to the evolution of the mesoderm and thereby before the origin of the notochord leaving their ancestral role largely unidentified.

1.6 Aims of the study.

The origin of the nervous system remains unresolved. One theory is that neurons originated from gland/secretory-like precursors (Brunet & Arendt, 2016; Moroz, 2009). The cnidarian *Nematostella* is a powerful model organism to try to illuminate this question due to its phylogenetically informative position as the sister group to bilaterians. Recent studies have shown that gland/secretory cells differentiate from *NvSoxB(2)* progenitor cells, but apart from this, little is known about the specification and differentiation of gland/secretory cells in *Nematostella*. Based on preliminary observations in the group, suggesting expression of *Nematostella Not* genes in neural and/or gland/secretory cells, this study aims (1) to elucidate the role of the *Nematostella Not* homeobox genes, and (2) to provide new insight into the specification of gland/secretory cells in *Nematostella* to allow better comparison to the development of neurons. To achieve these aims, we set out the following objectives:

1. Use *in situ* hybridization and transgenic reporter lines to study the expression of *NvNot* homeobox genes throughout development as well as characterizing the *NvNot*-expressing cells.
2. Generate mutant lines by CRISPR/Cas9 to study the function of *NvNotE*.

2 Materials

Table 2.1.1: Chemicals

Chemical	Formula /Abbrev.	Supplier	Cat. No.
4-(1,1,3,3-Tetramethylbutyl)phenyl-polyethylene glycol	Triton X-100	Sigma Aldrich	9002-93-1
4`,6-diamidino-2-phenylindole	DAPI	ThermoFisher	62248
Acetic Anhydride	$(CH_3CO)_2O$	Sigma Aldrich	45830
Agarose		Life Technologies	16500500
Bovine serum albumin	BSA	Sigma Aldrich	A4503
Citric acid	$C_6H_8O_7$	Sigma Aldrich	C0759
Diemethyl sulfoxide	DMSO	Sigma Aldrich	D8418
DIG RNA labelling mix		Sigma Aldrich	11277073910
di-Sodium hydrogen phosphate dihydrate	Na_2HPO_4 x 2 H_2O	Merck	1.06580.1000
Ethanol	CH_3CH_2OH /EtOH	Sigma Aldrich	1.00983
Ethylenediaminetetraacetic acid	EDTA	ThermoFisher	F9260G
Formaldehyde	CH_2O	Sigma Aldrich	252549
Formamide (deionized)	CH_3NO	Sigma Aldrich	F9037 / 47671
Glutaraldehyde	$C_5H_8O_2$	Sigma Aldrich	G7651
Glycerol	$C_3H_8O_3$	Sigma Aldrich	49781
Glycine		Sigma Aldrich	50046
Heparin sodium salt		Sigma Aldrich	H3149
Hoechst 33342		ThermoFisher	62249
Hydrogen peroxide	H_2O_2	Merck	K50794709911
L-Cysteine	$C_3H_7NO_2S$	Sigma Aldrich	W326305
Lithium Chloride	LiCl	ThermoFisher	9480G
Maleic Acid	$C_4H_4O_4$ / MA	Sigma Aldrich	M0375
Methanol	CH_3OH / MeOH	Sigma Aldrich	32213
Nitro-blue tetrazolium chloride/5-bromo-4-chloro-3'-indolyphosphate p-toluidine salt	NBT/BCIP	Sigma Aldrich	11681451001
Polyethylene glycol sorbitan monolaurate	Tween20	Sigma Aldrich	P9416
Proteinase K		Sigma Aldrich	P2308
Sodium Chloride	NaCL	Sigma Aldrich	S7653
Sodium citrate tribasic dehydrate	Na citrate	Sigma Aldrich	71402

Sodium dihydrogen phosphate monohydrate	NaH_2PO_4 x H_2O	Merck	1.06346.1000
Sodium dodecyl sulfate	$CH_3(CH_2)_{11}OSO_3Na$ / SDS	Sigma Aldrich	05030
Sodium hydroxide	NaOH	Merck	1.06462.1000
Triethanolamine	$C_6H_{15}NO_3$ / TEA	Sigma Aldrich	90279

Table 2.1.2: Commercial kits and reagents

Name	**Supplier**	**Cat. No.**	**Application**
Boehringer Blocking solution (BBS)	Sigma Aldrich	11096176001	Blocking for ISH
Click-iT® EdU Imaging Kit	ThermoFisher	C10337	Detecting DNA synthesis
Deoxyribonucleic acid, single stranded from salmon testes	Sigma Aldrich	D9156	Hybridization buffer
EnGen® sgRNA synthesis kit, S. Pyogenes	New England BioLabs	ES3322	sgRNA synthesis
Eva Green	Biotium	31000	Melt curve
GeneRuler DNA Ladder Mix	ThermoFisher	SM0331	Agarose gel electrophoresis
Goat serum	Merck	G9023	Blocking
MEGAscript® Kit (SP6, T7)	Ambion	11175025910	RNA synthesis
Prolong Gold (with DAPI)	ThermoFisher	P36931	Cell slide mounting
SYBR Safe® DNA gel stain	Life technologies	S33102	Agarose gel electrophoresis
TSA® Plus Blocking	Perkin Elmer	FP1012	Blocking for FISH
TSA® Plus Cyanine 3	Perkin Elmer	NEL744001KT	FISH
TSA® Plus fluorescein	Perkin Elmer	NEL741001KT	FISH
Wizard SV gel and PCR clean-up	Promega	A9281	PCR purification

Table 2.1.3: Primers

Primers	**Sequence (5'-3')**	**Use**
M13 primer Fwd	GTAAAACGACGGCCAG	Synthesis of probe template

M13 primer Rev	CAGGAAACAGCTATGAC	Synthesis of probe template
NotE seq fwd (1)	CGCTTTGGCCGAGAGATATAAC	Sequencing
NotE seq rev (1)	CTAATGCCTGCCAGTGGTTGTC	Sequencing
NotEmelt1fwd	CGCTTTACGTCTCAGACATGG	Melt curve sgRNA1/3 injected animals
NotEmelt1rev	GCACATATAGCATGGCGGATAG	Melt curve sgRNA1/3 injected animals
NotEmelt2fwd	CCGCCATGCTATATGTGCATG	Melt curve sgRNA2 injected animals
NotEmelt2rev	CGCGGATCCCCAGGATC	Melt curve sgRNA2 injected animals
NotEMut1rev	GAGACTTCAGTGCAGTCTTC	PCR checking double sgRNA injected animals
NotEMut2fwd	CTCAAAGGGTAATCATTTCAG	PCR checking double sgRNA injected animals
sgRNA1	ttctaatacgactcactataGATGAGCCACTGCACTGAATCgttttagagctaga	CRISPR/Cas9
sgRNA2	ttctaatacgactcactataGAGAGACACGCCCTATTCAACgttttagagctaga	CRISPR/Cas9
sgRNA3	ttctaatacgactcactataGGGTGTTATGCCATGGTAAGgttttagagctaga	CRISPR/Cas9
sgRNA6	ttctaatacgactcactataGAATGGCCGAGTCAAGAGCTAgttttagagctaga	CRISPR/Cas9

Table 2.1.5: Antibodies

Name	Type	Supplier	Species	Dilution	Cat. No.
Alexa Fluor® 647 phalloidin		ThermoFisher	*Amanita phalloides*	1:100	A22287
Anti-GFP mouse monoclonal	Primary	Abcam	Mouse	1:250	AB1218
Anti-Mouse Alexa fluor 488	Secondary	Invitrogen	Goat	1:200	A1101
Anti-Rabbit Alexa fluor 568	Secondary	Invitrogen	Goat	1:200	A110011
Anti-DsRed Polyclonal	Primary	TaKaRa	Rabbit	1:100	632496

Table 2.1.6: Instruments

Name	Supplier	Function
C1000 Thermal Cycler	BioRad	qPCR/melt curve

Centrifuge 5415 R	Eppendorf	Centrifuge of samples
ChemiDoc XRS+	BioRad	Gel-imaging
Eclipse TE2000-U	Nikon	Injection of fertilized eggs
FemtoJet 4i + CellTram Vario	Eppendorf	Injection of fertilized eggs
FV3000 Confocal Laser Scanning Microscope	Olympus	Imaging of fluorescent ISH and immunofluorescence
Leica SP5 confocal microscope	Leica Microsystem	Imaging of fluorescent ISH and Immunofluorescence
Mastercycler Nexus GSX1	Eppendorf	PCR
NanoDrop™ One Microvolume UV-Vis Spectrophotometer	Thermo Scientific	Quantifying and qualifying DNA/RNA samples
Nikon eclipse E800 compound microscope w/ Nikon Digital Sight DSU3 camera	Nikon Corporation	Imaging of colorimetric ISH

Table 1.1.7: Software

Name	**Developer**	**Purpose**
SnapGene 5.2	GSL Biotech LLC	Analyzing sequencing
Fiji	(Schindelin et al., 2012)	Image viewing
C100 Manager software	BioRad	qPCR/melt curve
Image Lab 5.1	BioRad	Gel imaging
Imaris 8.4.1	Oxford instruments	Image processing

2.2 Buffers and solutions

10x PBS
18.6 mM $NaH_2PO4 \times H_2O$
84.1 mM $Na_2HPO4 \times 2\ H_2O$
1.75 M NaCl

20x SSC (pH 7.0)
175.3 g/l NaCl
44.1 g/l Na citrate

1x PBTw	**1x PBTx**	**0.1x SSCT**	**2x SSCT**
1x PBS	1x PBS	0.5% (v/v)20x SSCT	10% (v/v) 20x SSCT
0.1%(v/v) Tween20	0.2% (v/v) TritonX-100	0.4% (v/v) Tween20	0.4% (v/v) Tween20

TNTw
0.1 M Tris-Cl pH 7.5
0.15 M NaCl
0.1% Tween20

TNTx
0.1 M Tris-Cl pH 7.5
0.15 M NaCl
0.2% Triton X-100

1x Maleic acid buffer (MAB, pH 7.5)
100mM Maleic acid
150mM NaCl

Hybridization Buffer (+) (Hyb+)
50% (v/v) Formamide
5x SSC
1% (v/v) SDS
0.1% (v/v) Tween-20
50 µg/ml Heparin
100 µg/ml Salmon sperm DNA
0,925% (v/v) Citric acid
H_2O

Hybridization Buffer (-) (Hyb-)
50% (v/v) Formamide
5x SSC
1% (v/v) SDS
0.1% (v/v) Tween-20
0,925%(v/v) Citric acid
H_2O

0.5 % blocking reagent/TNT for FISH
0.1 M Tris-Cl (pH 7.5)
0.15 M NaCl
0.5 % (v/v) Blocking reagent

10% blocking reagent/1x maleic acid buffer for ISH
10% (w/v) Blocking reagent
1x Maleic acid buffer

Washing after antibody: PBS-Tx-BSA
1x PBS
0.2% (v/v) Triton X-100
0.1% (w/v) BSA

Staining buffer: NTMT
100 mM NaCl
100 mM Tris-HCl (pH 9.5)
50 mM $MgCl_2$
0.1%(v/v) Tween-20

Genomic DNA Extraction buffer
10 mM Tris-HCl (pH 8)
1 mM EDTA
25 mM NaCl
200 µg/µl Proteinase K

3 Methods

3.1 *Nematostella* culture

Animals were kept in 1/3 filtered seawater (*Nematostella* medium; NM). Embryos were raised at 21°C and adult polyps were maintained at 18°C. Spawning was induced as previously described (Fritzenwanker & Technau, 2002). Eggs were fertilized for 30 minutes (mins) and subsequently dejellied in 3% (w/v) cysteine/NM (pH 7.4) until jelly is dissolved followed by washing in NM.

3.2 Fixation

Embryos were fixed at 12 hpf (early blastula), 16 hpf (blastula), 20 hpf (gastrula) 30 hpf (late gastrula), 48 hpf, (early planula), 72 hpf (planula), 96 hpf (late planula), and 7 dpf (primary polyp) in ice cold 0.25% (v/v) glutaraldehyde/3.7% (v/v) formaldehyde (in NM) for 90s, then incubated for one hour (hr) in 3.7% (v/v) formaldehyde (in PBTw) at 4°C while slowly rocking. Embryos were then washed four times in PBTw and dehydrated through a methanol series in PBTw [25%, 50%, 75%, 100% (v/v)]. Embryos were stored in methanol at -20°C. Fixation for immunofluorescence was performed using 3.7% (v/v) formaldehyde in PBTx for > 2hrs at 4°C, followed by washing four times in PBTx. Samples were stored in PBTx at 4°C until they were processed further.

3.3 Probe synthesis for *in situ* hybridization

pGEMT-easy plasmids containing all genes used in this study were already present in the lab. PCR amplification was performed using GoTaq® DNA Polymerase (M300) according to the manufacture's specifications. The 50 µl reaction consisted of 10 µl 5X GoTaq® reaction buffer, 3 µl $MgCl_2$, 1 µl dNTPs (10mM), 1.5 µl µM of each primer (10mM) (table 2.1.3.), 0.25 µl GoTaq® DNA Polymerase (250U/µl) and 5-10 ng of plasmid. The PCRs were run with an initial 2 min denaturation at 95°C, followed by 40 cycles of 30 s at 95°C, 30 s at 55°C and 1 min at 72°C, followed by a final 2 min extension at 72°C. An aliquot was ran on a 1% agarose gel to verify the size, and purified with Wizard® SV Gel and PCR Clean-Up System. An equal amount of membrane binding solution was added to the PCR product before it was loaded onto the column and centrifuged at 16,000 x g for 1 min. The column was washed twice with wash buffer before the DNA was eluted in nuclease free H_2O. RNA synthesis was performed using the MEGAscript™ SP6/T7 Transcription Kit. 20 µl reactions contained 1x RNA polymerase (SP6/T7), 1x reaction

Buffer (SP6/T7), 1x digoxigenin-labelling (DIG) or dinitrophenol (DNP) mix, and 1 µg of the purified PCR product and was left over night (O/N) at 37°C. 2 µl (20 U/µl) of TURBO DNAse was then added, and the sample was incubated at 37°C for 30 min to remove the original template. An equal amount of LiCl was added and the sample was put at -20°C for 30 min. The sample was purified by centrifugation at 4°C at 16,000 x g for 15 min, and the pellet was resuspended in 70% EtOH and centrifuged at 4°C at 16,000 x g for 5 min. The pellet was resuspended in nuclease-free H_2O and stored with an equal amount of deionized formamide at -20°C.

3.4 Colorimetric *in situ* hybridization (ISH)

Samples were rehydrated through a MetOH series in PBTw [75%, 50%, 25%, 0% (v/v)], and incubated in 10 µg/ml Proteinase K/PBTw for 5 mins at room temperature (RT), followed by two 5 min glycine washes (4 mg/ml glycine in PBT). They were then washed in 0.1% TEA/PBTw, followed by the addition of 0.25%, then 0.5% acetic anhydride in 0.1% TEA/PBTw for 5 min each, before three 5 min washes in PBTw. The samples were refixed in 3.7% formaldehyde/PBTw for 30 mins before five 5 min washes in PBTw. They were left at 60°C O/N in Hyb(+) buffer, before 1 ng/µl (in Hyb(+) buffer) of DIG-labelled probes was denatured at 90°C for 5 mins and an equal volume added to the samples for a final concentration of 0.5 ng/µl of probe and left for >60hr at 60°C. Samples were washed with a series of Hyb(-) in 2X SSCT [75%, 50%, 25%, 0% (v/v)] washes, followed by 30 mins in 0.2X SSCT and two 30 mins washes in 0.1x SSCT at 60°C. They were then washed in PBTw three times for 5 mins at RT, before blocking with 0.5% BBS (50% MAB, 50% PBTw) for 5 min at RT and then in 1% BBS/MAB for 2 hrs at RT. The samples were then incubated O/N with 1:4000 anti-digoxigenin alkaline phosphatase (Roche) in 1% BBS/MAB at 4°C. They were then washed ten times for 15 mins each in PBS-TX-BSA, followed by a one 1 min and two 10 mins NTMT washes. Signal was developed with the NBT/BCIP (1:100) in NTMT. After staining was completed, the samples were washed four times with NTMT, followed by three washes in H_2O, destaining in EtOH to remove unspecific staining, two washes in PBTw and stored in 87% glycerol at 4°C. Samples were imaged on a Nikon Eclipse E800 compound microscope with a Nikon Digital Sight DSU3 camera.

3.5 Fluorescence *in situ* hybridization (FISH)

Fixed samples were incubated in 2% H_2O_2/MeOH to eliminate endogenous hydrogen peroxidase activity. The ISH protocol (section 3.4.) was followed from rehydration until the last 0.1X SSCT step. During hybridization, samples were incubated with either digoxigenin (DIG) or dinitrophenol (DNP) labelled riboprobes (MEGAscript Kit, Ambion) at a concentration of 1 ng/µl. Following the 0.1X SSCT wash, samples were washed in a series of 0.1X SSCT in PBTw [75%, 50%, 25%, 0% (v/v)] for 10 mins each. They were then washed four times for 5 mins in TNTw, blocked in 0.5% TNTblock [0.5% blocking reagent (PerkinElmer)/TNT] for 1hr at RT before incubation with anti-DNP-HRP (1:250, Roche) O/N at 4°C. They were then washed ten times for 15 min in TNTx at RT and incubated in Cyanine 3 (1:50) in 1X working solution (TSA Plus Kit, PerkinElmer) for 30 mins at RT. They were then washed two times for 5 mins in TNTw followed by a 5 min wash in PBTw. To stop peroxidase activity, samples were incubated in 0.1 M glycine (0.1% tween, pH 2) for 10 mins followed by 1 hr in 2% H_2O_2/PBTw. Subsequently, the samples were washed three times for 5 mins in TNTw at RT, blocked in 0.5% TNTblock [0.5% blocking reagent (PerkinElmer)/TNT] for 1 hr at RT, and incubated with anti-DIG-POD (1:100, Roche) O/N at 4°C. They were then washed ten times for 15 min in TNTx before incubation in fluorescein (1:50) in 1X working solution (TSA Plus Kit, PerkinElmer) for 30 mins at RT. They were then washed two times for 5 mins in TNTx and 5 mins in PBTx. The samples were incubated in Hoechst/PBTx (1:100) for 1 hr to stain DNA. They were then washed four times in PBTx before mounted in ProLong Gold (with DAPI) antifade reagent. Samples were image on an Olympus FV3000 Confocal Laser Scanning Microscope or a Leica SP5 confocal microscope and processed in Imaris or Fiji (Schindelin et al., 2012).

3.5.1 EdU staining

Samples were incubated for 30 mins in 100 µM EdU in NM (Click-iT® EdU Imaging Kit) before they were fixed as above (section 3.5.). The samples were processed following the FISH protocol until the first TSA reaction. They were then washed in 3%BSA/PBS for 15 mins at RT, before the samples were incubate for 30 mins in freshly made reaction cocktail [430 µl 1X Click-iT® reaction buffer, 20 µl $CuSO_4$ (100 mM), 1.2 µl Alexa Fluor® azide, 50 µl 1X Click-iT® EdU buffer additive].

They were subsequently washed three times for 10 mins in PBTx before they underwent DNA staining and mounting as above (section 3.5.).

3.6 Immunofluorescence

Fixed animals to undergo immunostaining were first in block (5% goat serum/ 3% BSA/ PBTx) for 1 hr at RT, before O/N incubation in primary antibody in block at 4°C (table 2.1.5). Samples were subsequently washed several times for a total of 2h in PBTx, incubated for 1 hr in block and secondary antibody and phalloidin in block O/N at 4°C (table 2.1.5.). The samples were subsequently incubated in Hoechst (1:100) in PBTx for 1 hr, washed several times in PBTx for a total of 2 hrs and then mounted in ProLong Gold (with DAPI) antifade reagent. Samples were image as above (section 3.5).

3.7 CRISPR/Cas9 mediated mutagenesis

CRISPR/Cas9 allows genome editing based on RNA guided endonuclease activity (Ikmi et al., 2014). This requires the synthesis of single guide RNAs (sgRNA) to target a 20 bp target sequence. Cas9 will cut the DNA at its target location. As the cells own repair system, Non-homologous End Joining (NHEJ), is error prone, this will lead to the introduction of mutations. SgRNAs were designed (table 2.1.3.) and synthesized following the EnGen sgRNA synthesis kit protocol (NEB). A 20 µl reaction mix consisted of 10 µl 2X sgRNA reaction mix (*S. pyogenes*), 5 µl target specific designed DNA oligo (1 µM), 1 µl DTT (0.1 M), 2 µl EnGen sgRNA enzyme mix. The mixture was incubated at 37°C for 1 hr before the volume was increased to 50 µl with nuclease-free H_2O and 2 µl DNase I mix (NEB) was added and incubated at 37 °C for 15 mins. An equal volume of LiCl was added and the RNA was purified as described above (section 3.3). The purified RNA was stored without formaldehyde at -80°C. The injection mix, consisting of 500 ng/µl Cas9 enzyme (PNA Bio CP01), 112.5 ng/µl of sgRNA, and 25% (v/v) Alexa dextran fluorescent dye (in 1.1 M KCl) was incubated at 37°C for 5 min prior to injection. The injection mix was microinjected according to previously published protocols (Rentzsch et al., 2020). Injected animals were grown to primary polyp stage (approx. 10 dpf) before genomic DNA was extracted from a subset of the animals to check for the presence of mutations. DNA was extracted by adding 100% EtOH to tubes with polyps and incubated for 5 mins. The EtOH was then removed, and the samples were incubated

for 45 mins at 50°C before they were incubated in genomic extraction buffer for 2 hrs at 50°C followed by 10 mins at 98°C to inactivate the proteinase K and stored at 4°C. For double sgRNA injected animals PCR with standard Q5 DNA polymerase, followed by 1% agarose gel electrophoresis was used to check for mutants, otherwise a melt curve reaction was performed (section 3.8). For sgRNAs, or combinations thereof, where mutations were detected in these F0 animals, the remaining injected animals were raised to sexual maturity. They were then individually crossed to wildtypes and the resulting F1 animals were analyzed (by both melt curve/gel electrophoresis and sequencing) to identify F0 animals carrying desirable mutations.

3.8 Melt curve with EvaGreen®

A PCR was performed on a 100 bp amplicon centered on the predicted sgRNA cut site. This is performed in the presence of an intercalating dye (EvaGreen) that fluoresces when bound to double stranded DNA. The PCR is then followed by a denaturing stage coupled to the reading of the fluorescence to measure the melting temperature of the amplicon. Mutations will lead to changes in this temperature leading to observable changes in the resulting melt curves. A 30µl Q5 reaction was assembled with 6 µl 5X Q5 buffer, 0.75 µl dNTPs (10mM), 1 µl fwd and rev primer (10 mM) (table 2.1.3.), 0.25 µl Q5 High-Fidelity DNA Polymerase (2.5 U/µl), 1.5 µl 20X EvaGreen® Dye and 2 µl genomic DNA. The PCR were run with an initial 1 min denaturation at 98°C, followed by 40 cycles of 10s at 98°C, 30s at 60°C and 30s at 72°C, followed by a final 2 min extension at 72°C. The samples were then analyzed in a C1000 Thermal Cycler (BioRad) with a starting temperature at 60°C, followed by a 0.5°C incremental increase in temperature followed by reading of fluorescence until it reaches 95°C.

3.9 Sequencing

The genomic DNA was sequenced by standard Q5 PCR reaction with the extracted genomic DNA as template (table 2.1.3.). An amplicon was designed for approx. 500 bp surrounding the Cas9 cut site. The PCRs were run with initial 30s denaturation at 98°C, followed by 40 cycles of 10s at 98°C, 15s at 60°C and 1 min at 72°C, followed by a final 2 min extension at 72°C. The PCR product was diluted 1:10 and 5 µl was added to 2.5 µl H_2O and 2.5 µl of primer (10mM) before being sent for Sanger sequencing (GENEWIZ). Results were analyzed in SnapGene.

4. Results

The main aim of this thesis is to investigate the role of *Not* homeobox genes in the context of cell specification in the sea anemone *Nematostella vectensis*. A microarray experiment was previously performed to identify genes involved in neurogenesis and/or gland/secretory cell development. This was done by comparing the gene expression under two conditions: embryos injected with *NvSoxB(2)* morpholino and embryos treated with DAPT resulting in downregulation and upregulation of neurogenesis and potentially gland/secretory cell development, respectively (G.S. Richards, J. Blommaert and F. Rentzsch, unpublished). From this an extensive list of candidate genes was generated. The homeobox genes *NvNotA* (Nve 123835), *NvNotC* (Nve 4967) and *NvNotE* (Nve 2174) were looked at closer by a preliminary colorimetric *in situ* and their expression pattern was deemed interesting for further analysis.

4.1 Characterization of the developmental expression patterns of Not genes

In situ hybridization (ISH) is used to look at the specific localization of mRNA within an embryo and is thereby an intuitive starting point for the characterization of a gene. Using *in situ* hybridization (ISH), the aim was to establish a spatial and temporal expression pattern of *NvNotA*, *NvNotC*, and *NvNotE*. Further, double fluorescence *in situ* hybridization (DFISH) was used to better characterize the identity of these cells by investigating co-expression with other cell markers.

4.1.1 *NvNotA* and *NvNotC* are expressed in scattered cells during development

First, *in situ* hybridization was performed to analyze the expression of *NvNotA*, *NvNotC* and *NvNotE* (Section 3.4). *NvNotA* expression is not visible until planula stage when it starts to be expressed in scattered cells in the mesendoderm (Figure 4.1 A-E, G-K). This is also observed for late planula stages (Figure 4.1 F, L). No expression is visible for *NvNotC* at blastula stage (Figure 4.1 M, S). Expression starts at gastrula stage in a small number of cells in the ectodermal epithelium (Figure 4.1 N, T). At late gastrula, the *NvNotC*-expressing cells (*NvNotC*$^{+}$) are greater in number and are largely restricted to the aboral pole (Figure 4.1 O, U). At early planula, cells expressing *NvNotC* can be observed in the forming pharynx (indicated by arrow, Figure 4.1 P),

and from planula, expression of *NvNotC* can also be observed in the mesendoderm (indicated by arrow, Figure 4.1 Q) with some cells in the ectoderm (indicated by arrow, Figure 4.1 R, W-X).

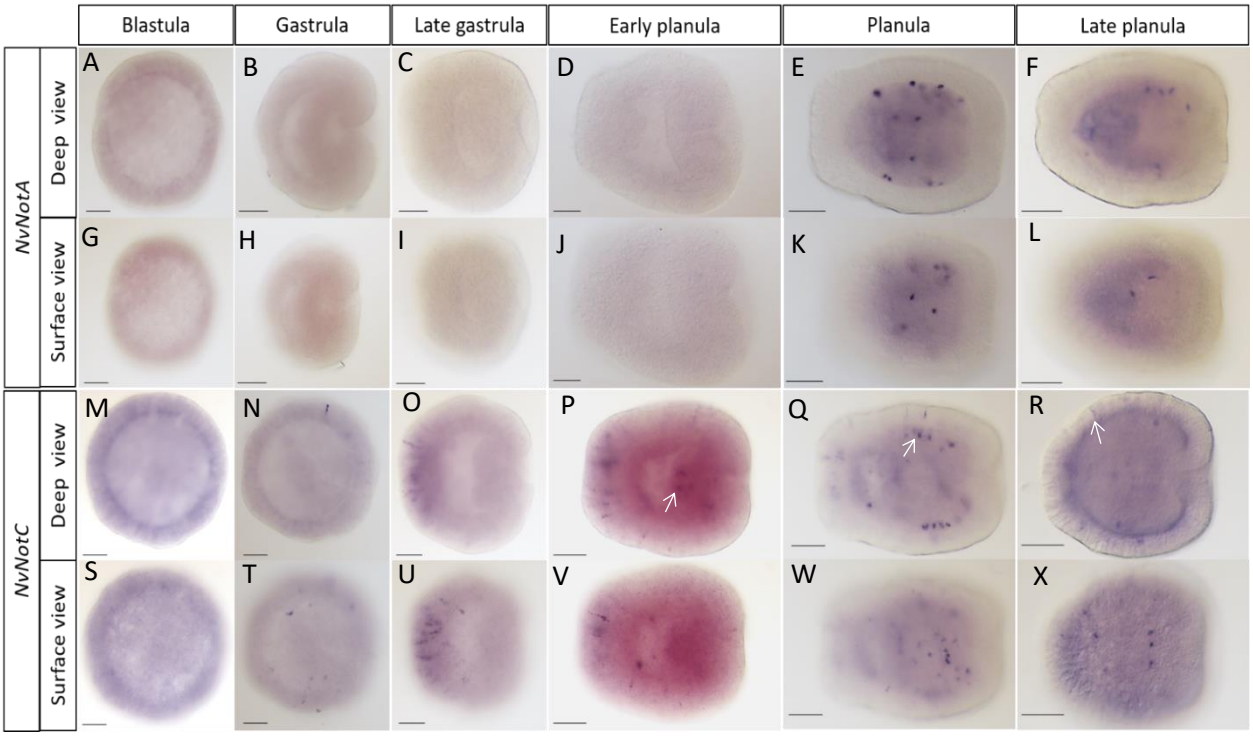

Figure 4.1: Expression patterns of *NvNotA* and *NvNotC*. *In situ* hybridization of *NvNotA* and *NvNotC* with developmental stages indicated on the top, and gene names on the left. The embryos are oriented with their oral pole to the right. (A-F, M-R) show the middle of the embryo. (G-L, S-X) is focused on the surface of the embryos. At blastula stage (16hpf) throughout early planula (48hpf) no expression of *NvNotA* can be observed (A-C, G-H). At planula (72hpf) and late planula (96hpf), *NvNotA*-expressing cells can be observed in the mesendoderm (E-F, K-L). expression of NvNotC is initiated at gastrula stage (20hpf) with few cells in the epithelium (M, S). At late gastrula (30hpf), more *NvNotC*-expressing cells are appearing at the aboral pole (O, U), and at planula stages expression can be observed in cells in the mesendoderm (white arrow, Q), the forming pharynx (white arrow, P) and a few distinct cells in the ectoderm (P-R, V-X). Scale bars: 50µm

To summarize, *NvNotA* is expressed in the mesendoderm from planula stage, while *NvNotC*-expression starts at gastrula and is expressed in the aboral ectoderm at late gastrula. At planula *NvNotC*$^{+}$ cells are found in the mesendoderm and in few ectodermal cells.

4.1.2 *NvNotE* is expressed in *NvMucin* expressing gland cells

ISH was also performed for *NvNotE*, which showed that expression of *NvNotE* starts at blastula stage with few scattered cells (Figure 4.2 A, G). At gastrula and late gastrula, the number of *NvNotE*-expressing cells increases and is restricted to the aboral pole (Figure 4.2 B-C, H-I). At early planula stage, expression is also seen in the pharynx (Figure 4.2 D, J). This pattern persists through planula and late planula stage (Figure 4.2 E-F, K-L). The *NvNotE* expression pattern resembled

that of known neural or gland cell markers, and in the *Nematostella* single cell atlas, *NvNotE* was identified to be present in a gland/secretory *NvMucin* expressing metacells (Sebé-Pedrós et al., 2018). Mucins are large glycoproteins abundant in gland/secretory cells (Levitan et al., 2015). To compare the expression patterns of *NvNotE* and *NvMucin,* ISH was performed for *NvMucin* (Figure 4.2 M-Y). Expression of *NvMucin* starts at the same time as *NvNotE,* with weak expression at blastula stage (Figure 4.2 M, S). At gastrula stage, expression is observed in the aboral ectoderm (Figure 4.2 N, T). At late gastrula stage, *NvMucin*-expressing cells can be observed towards the oral pole in addition to a high number of *NvMucin*-expressing cells at the aboral pole (Figure 4.2 O, U). Similarly to *NvNotE*, at early planula there are cells expressing *NvMucin* starting to appear along the pharynx which persist throughout the planula stages (Figure 4.2 P-R, V-X). At primary polyp, NvMucin is expressed in cells in the tentacles, in the pharynx and in the ectoderm (Figure 4.2 Y-Y'').

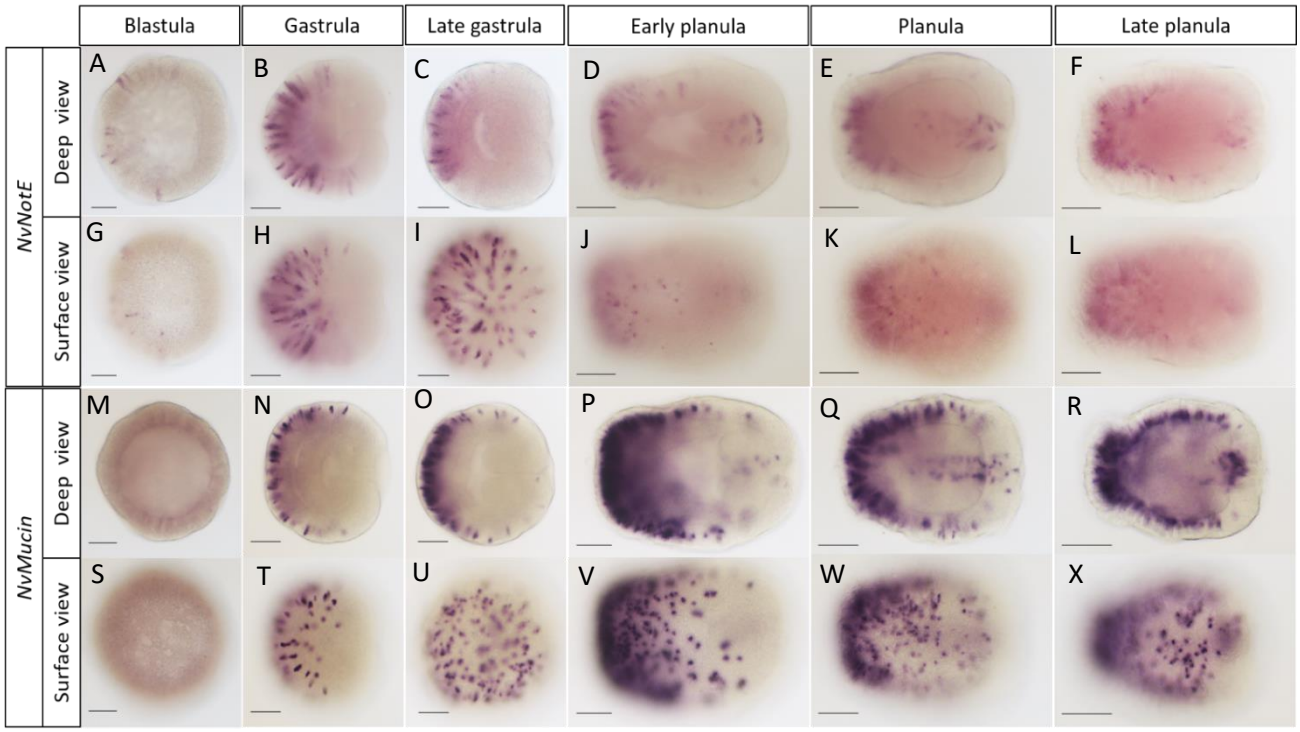

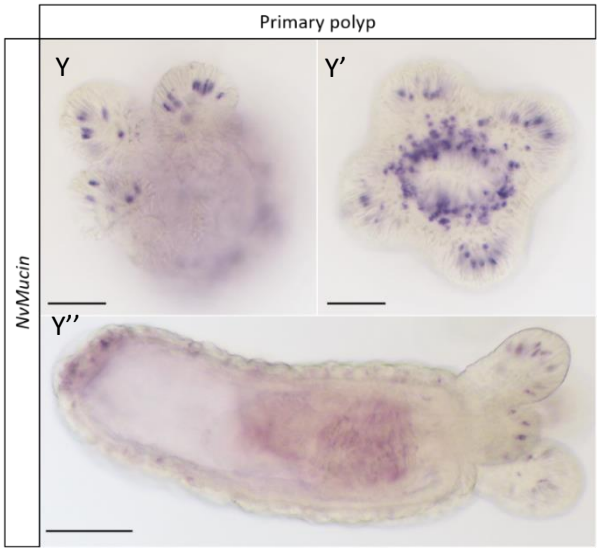

Figure 4.2: *NvNotE* and *NvMucin* show similar expression pattern. *In situ* hybridization of *NvNotE* and *NvMucin*. Developmental stages are indicated on the top, and gene names on the left. Embryos are oriented with their oral pole to the right. (A-F, M-R) show the middle of the embryo. (G-L, S-X) is focused on the surface of the embryo. Expression of *NvNotE* initiates at blastula stage (16hpf) in few epithelial cells (A, G). At gastrula (20hpf) and late gastrula (30hpf) the number of *NvNotE*-expressing cells increases and is restricted to the aboral pole (C-D, I-J). At early planula (48hpf) and late planula (96hpf), cells expressing *NvNotE* are observed at the aboral pole and in the forming pharynx (D-F, J-L). Weak *NvMucin* expression is observed at blastula stage (M, S), with stronger expression observed at the aboral pole for gastrula stage (N, T). At late gastrula, the number of *NvMucin*-expressing cells increases (N, T), and at early planula cells expressing *NvMucin* appear in the pharynx (P, V). This expression pattern is maintained in planula (72hpf) and late planula stages (Q-R, W-X). Primary polyp (7dpf) shows expression of NvMucin in the

Based on the expression pattern of *NvNotE*, the similarity to the *NvMucin* expression and the presence of an already existing *NvNotE*::GFP transgenic line, we decided to focus on *NvNotE* for further investigation.

4.1.3 *NvNotE* is expressed in non-proliferating cells

To investigate whether *NvNotE* is expressed in proliferating cells, embryos at gastrula and planula stage were exposed to 30 min labeling of EdU before they were immediately fixed (Section 3.5.1). EdU is a thymidine analog that is incorporated during DNA replication and therefore allows the identification of proliferating cells (Chehrehasa et al., 2009). They subsequently underwent fluorescence *in situ* hybridization (FISH) and EdU detection. Four embryos of each developmental stage were investigated and there was no finding of *NvNotE*$^{+}$ cells that incorporated EdU at gastrula or planula stage (Figure 4.3). This suggest that *NvNotE* is mostly expressed in non-proliferating cells.

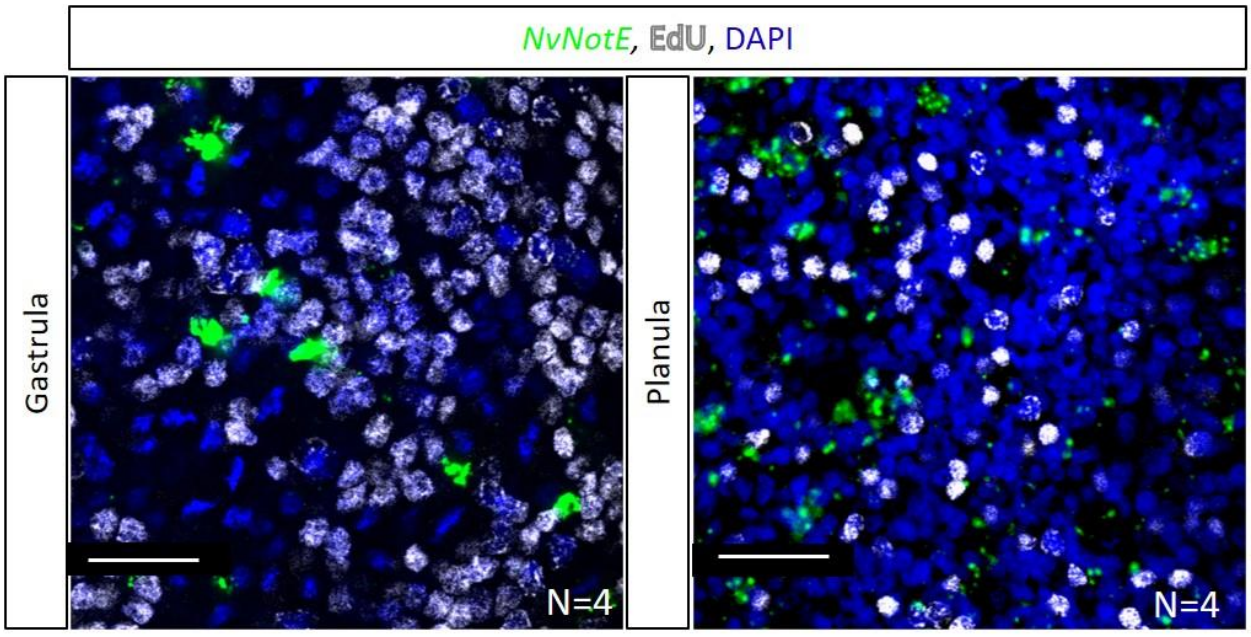

Figure 4.3: *NvNotE* is expressed in non-proliferating cells. Fluorescence *in situ* hybridization of *NvNotE* (green), with Click-iT EdU detection (grey) and DAPI (blue), at gastrula and planula stage. Developmental stages are indicated to the left with the staining indicated at the top. No *NvNotE*$^{+}$ cells were observed incorporating EdU after 30 min pulse labelling. "N" indicates the number of animals analyzed. Scale bars: 20 µm.

4.1.4 *NvNotE* is co-expressed with *NvSoxB(2), NvMucin* and *NvInsm1*

To better characterize the identity of *NvNotE*-expressing cells, co-expression experiments were performed by double fluorescence *in situ* hybridization (DFISH, Section 3.5). First, DFISH was performed with *NvSoxB(2)*, a marker of progenitor cells (Figure 4.4 A-F''). *NvNotE* was co-expressed with *NvSoxB*(2) in a few cells at gastrula stage (Figure 4.4 A-B''), but the majority of

cells express only one of the two genes. No co-expression was observed at early planula or planula stage (Figure 4.4 C-F''). As *NvNotE* was suggested to be expressed in *NvMucin* expressing gland/secretory cells, co-expression between the two was investigated. *NvMucin* and *NvNotE* are co-expressed in most cells observed for both gastrula, early planula, and planula stages at the aboral pole and in the pharynx (Figure 4.4 G-L''), however the co-expression is not absolute as there are cells only expressing *NvMucin*. Though, most *NvNotE*$^{+}$ cells also express *NvMucin*. DFISH was also performed with *NvNotE* and *NvInsm1*, the latter recently having been shown to be expressed in neurons and gland/secretory cells, including *NvMucin*$^{+}$ cells (Tournière et al., 2021). Co-expression can be observed at all three developmental stages analyzed, with most *NvNotE*$^{+}$ cells expressing *NvInsm1*, while many cells expressing only *NvInsm1*$^{+}$ were observed (Figure 4.4 M-R'').

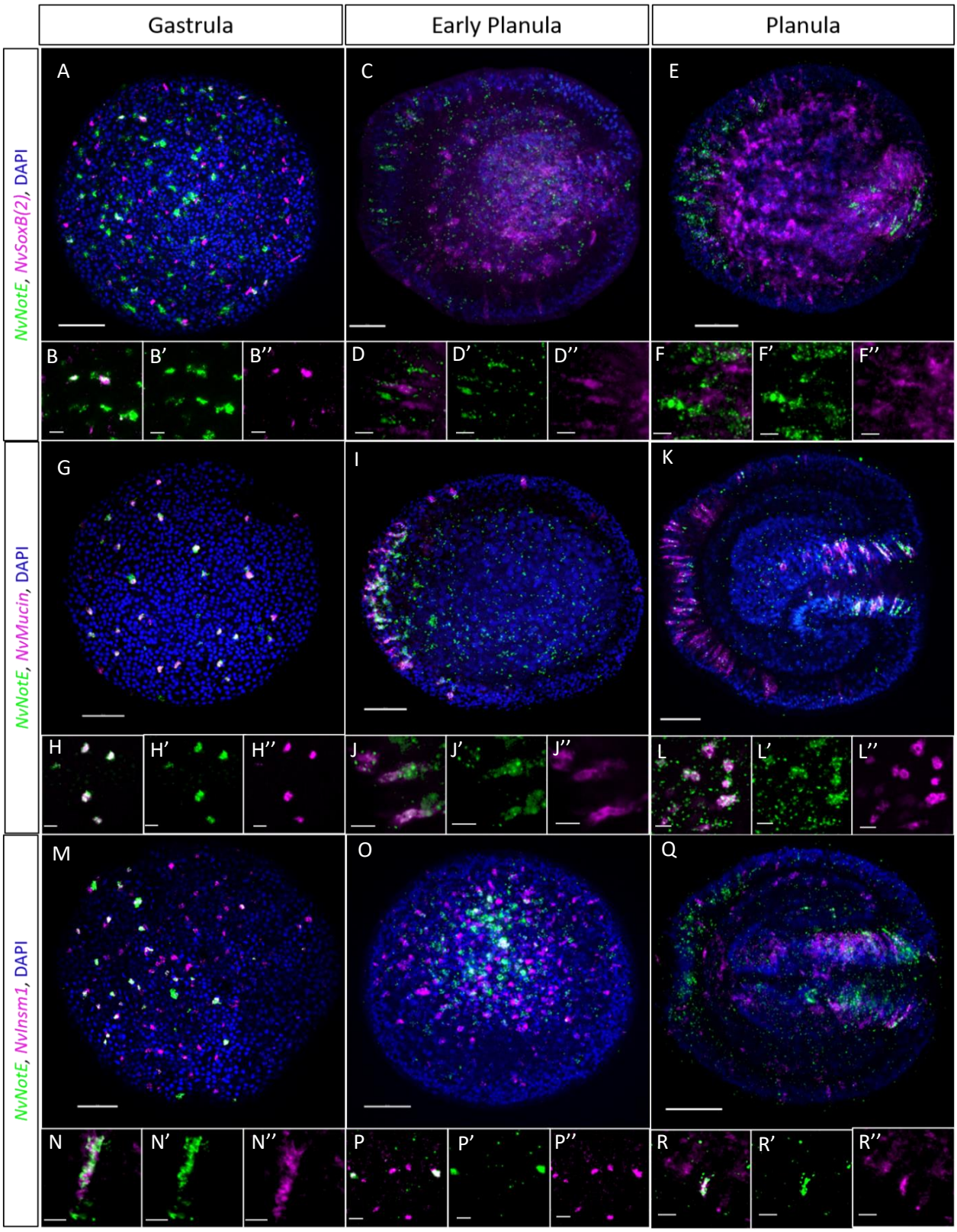

Figure 4.4: *NvNotE* is partially co-expressed with *NvSoxB*(2), *NvMucin* and *NvInsm1*. Double fluorescence *in situ* hybridization for *NvNotE* (green) with either *NvSoxB*(2), *NvMucin,* and *NvInsm1* (magenta). Developmental stages are shown on the top and genes are shown to the left. Embryos are oriented with their oral pole to the right. Neural progenitor marker *NvSoxB(2)* shows partial co-expression with *NvNotE* at gastrula (20hpf) (A, B). At early planula (48hpf) and planula (72hpf) no co-expression is observed (C-F). Gland/secretory marker *NvMucin* shows co-expression with *NvNotE* in all developmental stages investigated (G-L). Most *NvNotE*$^{+}$ cells appear to express *NvMucin*$^{+}$. *NvInsm1*, expressed in both neurons and gland/secretory cells, is co-expressed with *NvNotE*$^{+}$ at gastrula, early planula, and planula (M-Q). DAPI is shown in blue. All images are single confocal sections. Scale bars: 50 µm (A, C, E, G, I, K, M. O, Q), 10 µm (B, D, E, F, H, J, N, P, R).

To further characterize the identity of *NvNotE*-expressing cells, co-expression with a broad array of genes was investigated (Figure 4.5). No co-expression of *NvNotA* or *NvNotC* with *NvNotE* at planula stage was detected (Figure 4.5 A, B). The observed co-expression with *NvMucin* and *NvInsm1* might suggest a role in gland/secretory cells. To further investigate this, DFISH was performed with *NvTrypsinA* and *NvIlp2*, both expressed in gland/secretory cells (Steinmetz et al., 2017). No co-expression with *NvNotE* was detected at planula stage (Figure 4.5 C, D). *NvNcol3* encodes the Ncol3 protein found in the capsule wall of cnidocytes (Zenkert et al., 2011). *NvNcol3* and *NvNotE* show no co-expression at planula stage (Figure 4.5 E). *NvLWamide* and *NvRFamide* are neuropeptides expressed in neurons. No co-expression with *NvNotE* is observed for either at planula stage (Figure 4.5 F-G). *NvFoxQ2d* is found in scattered sensory neurons. DFISH performed at early planula showed no co-expression of *NvFoxQ2d* and *NvNotE* (Figure 4.5 H).

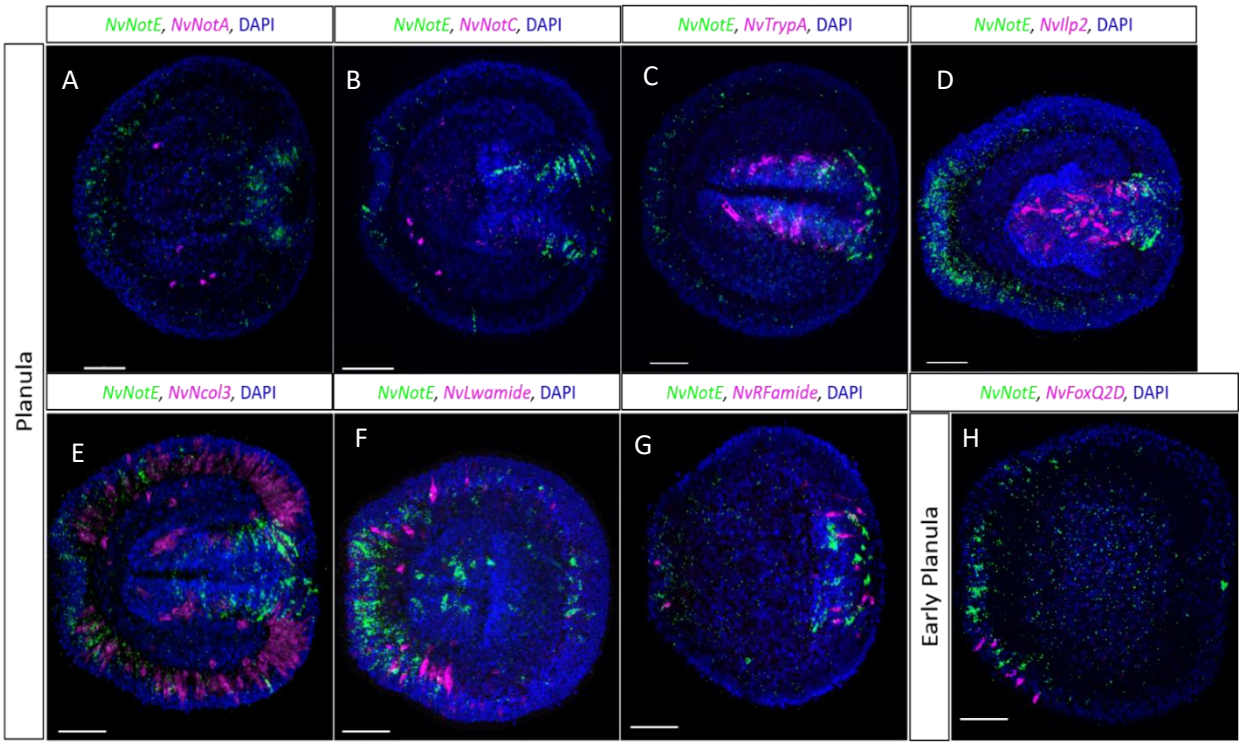

Figure 4.5: Double fluorescence *in situ* hybridization to characterize the identity of *NvNotE*-expressing cells. *NvNotE* (green) with either *NvNotA*, NvNotC*, NvIlp2*, *NvTrypA*, , *NvNcol3*, *NvLWamide*, *NvRFamide* or *NvFoxQ2d* (magenta). Developmental stages are shown to the left with genes shown on the top. Embryos are oriented with their oral pole to the right. *NvNotA* (A) and *NvNotC* (B) show no co-expression with *NvNotE* at planula (72hpf). The gland/secretory markers *NvTrypA* (C) and *NvIlp2* (D) show no co-expression with *NvNotE*. No co-expression between cnidocyte marker *NvNcol3* and *NvNotE* is observed (E). Neuropeptides *NvLWamide* (F) and *NvRFamide* (G) is not observed to be expressed in *NvNotE*$^{+}$ cells at planula. Finally, putative sensory cell marker, *NvFoxQ2d*, is not co-expressed with *NvNotE* at early planula stages (48hpf). All images are single confocal sections. DAPI is shown in blue. Scale bars: 50µm.

To summarize, expression of *NvNotE* is initiated at the aboral pole at blastula stage, and at planula stage *NvNotE*$^{+}$ cells are found in the aboral ectoderm and in the pharynx. *NvNotE* is partially co-expressed with progenitor marker *NvSoxB(2)* and *NvInsm1*, expressed in neurons and gland/secretory cells. *NvNotE* was also identified to be present in gland/secretory *NvMucin*-expressing cells.

4.2 *NvNotE*-expressing cells develop into gland/secretory cells

With the temporal and spatial expression pattern established, it was interesting to investigate the nature of *NvNotE*$^{+}$ cells. To do this, a transgenic line was used. The ability to generate stable transgenic lines in *Nematostella* is an important tool to determine cell identity. It allows visualization of a cell's morphology even after the gene expression is terminated, thereby allowing to trace the progeny of a cell. Crossing of *NvNotE*::*GFP* transgenic line to characterized reporter lines, analyzed by immunocytochemistry (Section 3.6), helps illuminate the identity of *NvNotE*-expressing cells.

4.2.1 A transgenic reporter line gives insight to the nature of *NvNotE*-expressing cells

A transgenic reporter line with regulatory elements of the *NvNotE* gene driving the expression of GFP had already been generated in the lab. To gain further insight into the nature of *NvNotE*-expressing cells, GFP expression was analyzed. Expression of the transgene resembles the expression pattern found with ISH (Figure 4.2). At gastrula, GFP is localized in scattered ectodermal elongated cells, some appearing to have an apical cilium. Vesicle-like structures are observed in cells expressing the transgene (Figure 4.6 A, H). At late gastrula and early planula, the transgene is expressed in aboral cells with rare *NvNotE*-transgene expressing cells closer to the oral pole (Figure 4.6 B). At planula and late planula, there is still a high number of aboral cells spanning the ectoderm, however more cells expressing the transgene are observed at the oral pole and in the pharynx at late planula stage (Figure 4.6 D, E). At primary polyp, *NvNotE*::GFP-expressing cells are found as elongated cells in the tip of the tentacles, at the aboral pole, and in cells spanning the ectoderm of the body column with some having processes (indicated by arrow, Figure 4.6 F, G, I). Cells expressing the transgene are also present in the pharynx (indicated by white bracket, Figure 4.6 F, G).

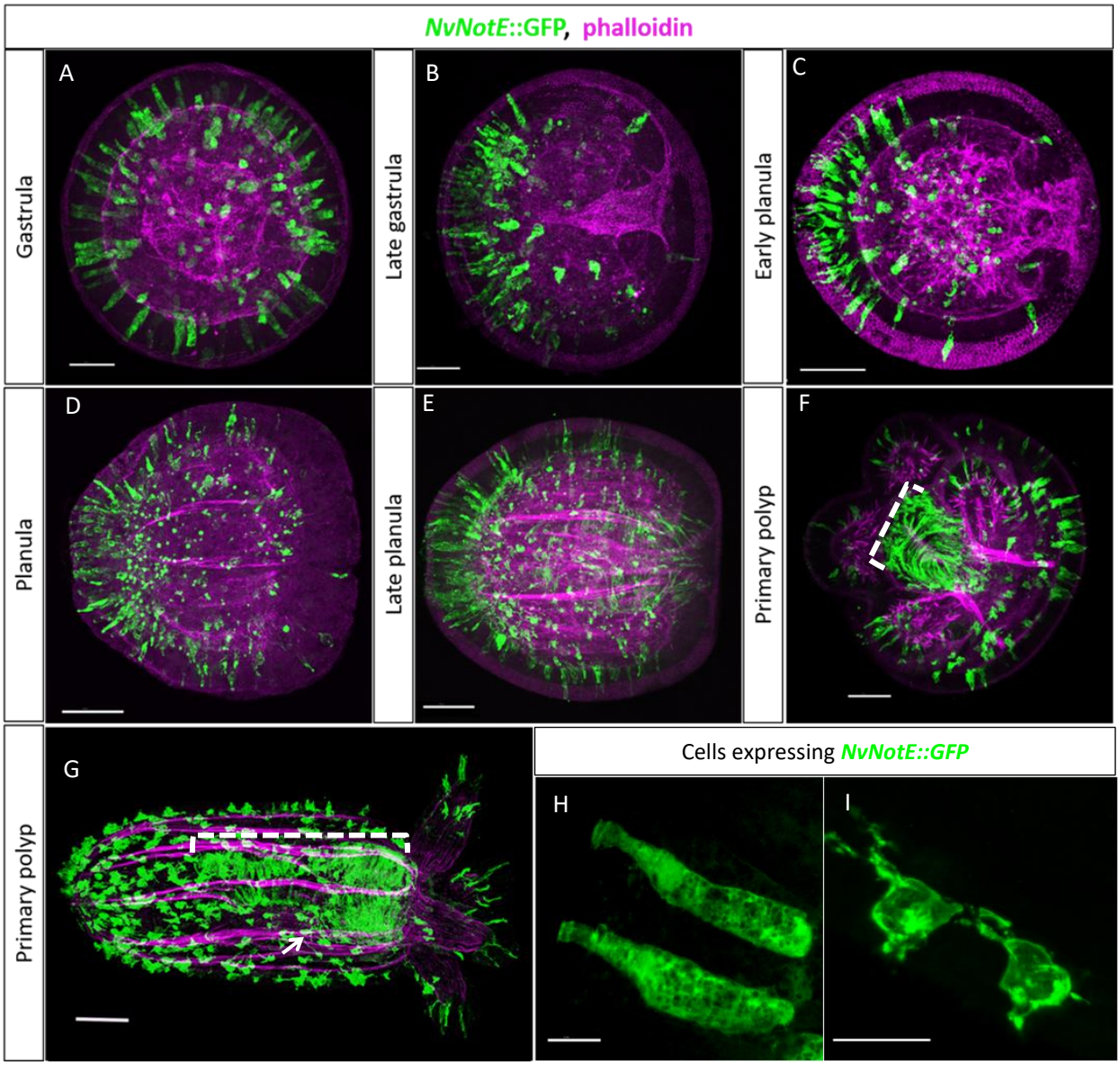

Figure 4.6: A transgenic reporter line reveals *NvNotE*$^{+}$ cell morphology. *NvNotE*::*GFP* transgenic line detected by anti-GFP antibody (green) and phalloidin staining of F-actin (magenta). Developmental stages are indicated to the left. Animals are oriented with the oral pole to the right, except for (F) where the oral pole is facing forward/top left corner. At gastrula stage (20hpf), cells expressing the transgene can be observed in the ectoderm in elongated cells (A). At late gastrula stage (30hpf), and early planula (48hpf), *NvNotE*$^{+}$ cells are visible at the aboral pole with few *NvNotE*-expressing cells towards the oral pole (B-C). At planula stage (72hpf), expression of GFP is found in increasing number of cells towards the oral pole (D), and by late planula (96hpf) elongated cells expressing the transgene are visible in the pharynx. At primary polyp *NvNotE*::GFP cells are found as elongated cells at the aboral pole, in cells in the ectoderm along the body column, with some having processes indicated by a white arrow (G). Cells expressing the transgene are also present in the tip of the tentacles and in the oral opening and pharynx (G, F). White brackets indicate the pharynx (F, G). Cells expressing *NvNotE*::GFP containing vesicle-like structures at gastrula (H), and *NvNotE*::GFP-expressing cells found in the body column at primary polyp stage (I) All images are 3D reconstructions. Scale bars: 50 µm (A-G), 10 µm (H-I)

4.2.2 *NvNotE::GFP* expressing cells also express *NvSoxB(2)::mOrange* early in development

To further investigate the relationship between *NvNotE* and *NvSoxB*(2)-expressing progenitor cells, double transgenic animals were generated by crossing *NvNotE::GFP* to the *SoxB(2)::mOrange* reporter line. At gastrula stage *NvNotE::*GFP-expressing cells can also be found expressing the *NvSoxB(2)* reporter transgene (Figure 4.7 A-B''). There are more cells exclusively expressing the *NvSoxB(2)*-transgene than the *NvNotE*-transgene. From early planula to primary polyp, cells expressing both transgenes were not observed (Figure 4.7 C-J'').

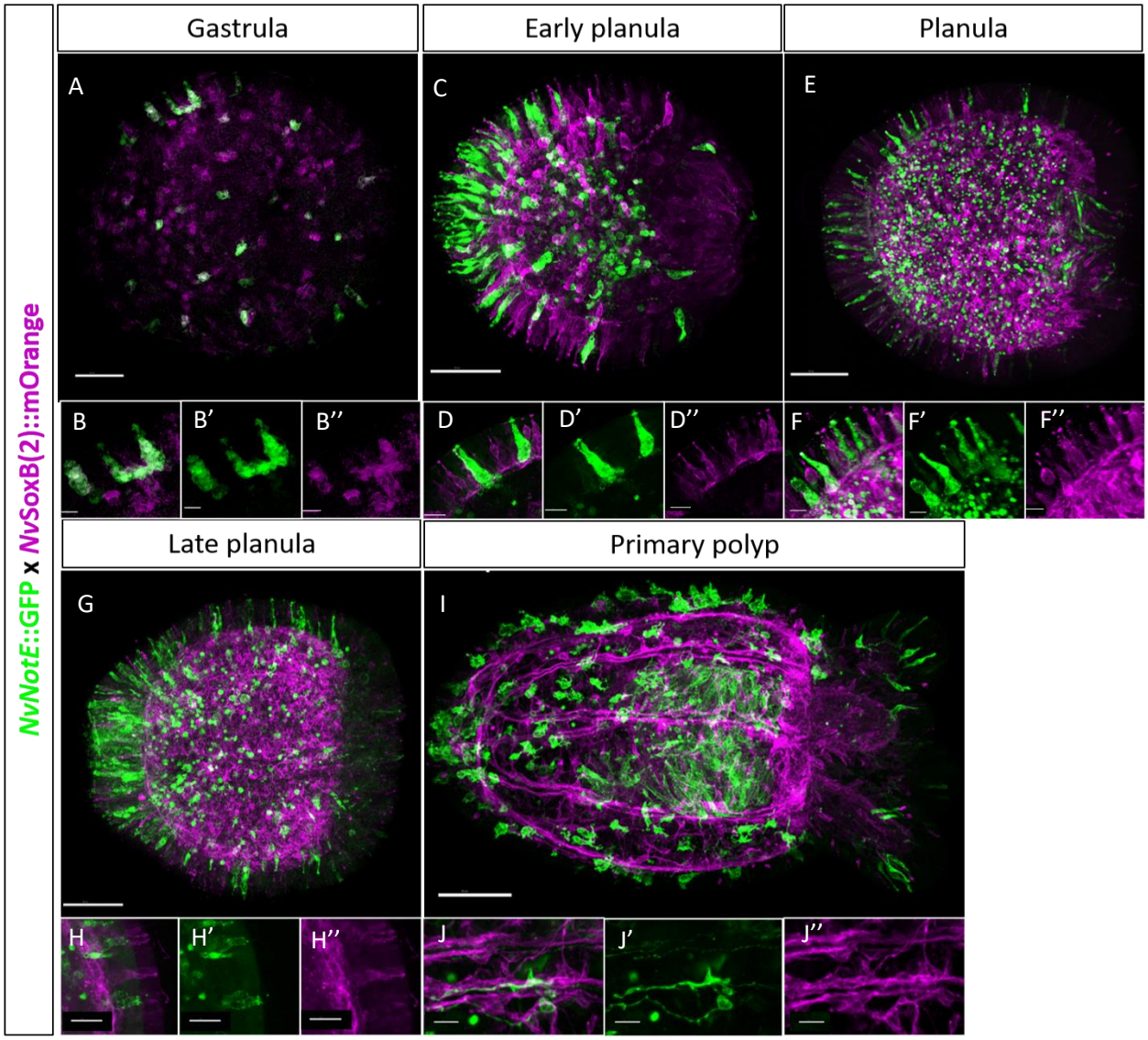

Figure 4.7: *NvNotE*::GFP cells express the *NvSoxB(2)* transgene at gastrula stage. Double transgenic animals with *NvNotE*::GFP (green) crossed with *NvSoxB(2)*::mOrange (magenta). Transgenes are indicated to the left. Developmental stages are shown on the top. Animals are oriented with their oral pole to the right. At gastrula stage (20hpf), cells labelled by the *NvNotE* transgene are also labeled by the *NvSoxB(2)* transgene in selected cells (A-B''). At early planula stage (48hpf), planula (72hpf), late planula (96hpf) and primary polyp (7dpf), *NvNotE*-transgene expressing cells are not found to express the *NvSoxB(2)* transgene (C-I''). All images are 3D reconstructions. Scale bars: 50 µM (A, C, E, G, I), 10 µM (B, D, F, H, J)

4.2.3 *NvPOU4::mOrange* labelled cells do not express *NvNotE*

The *NvPOU4*::*mOrange* transgenic line labels post mitotic neurons and cnidocytes (Tournière et al., 2020). *NvNotE* was not co-expressed with cnidocyte marker *NvNcol3* by DFISH (Figure 4.5 E). However, the *NvPOU4*::*mOrange* reporter line was found to not only label cnidocytes, but also sensory and ganglion cells (Tournière et al., 2020). To investigate if *NvNotE*::GFP is expressed in a subset of *NvPOU4::*mOrange labelled cells, double transgenic animals were generated. Co-expression of mOrange and GFP was not observed at gastrula or planula stage (Figure 4.8 A-D'').

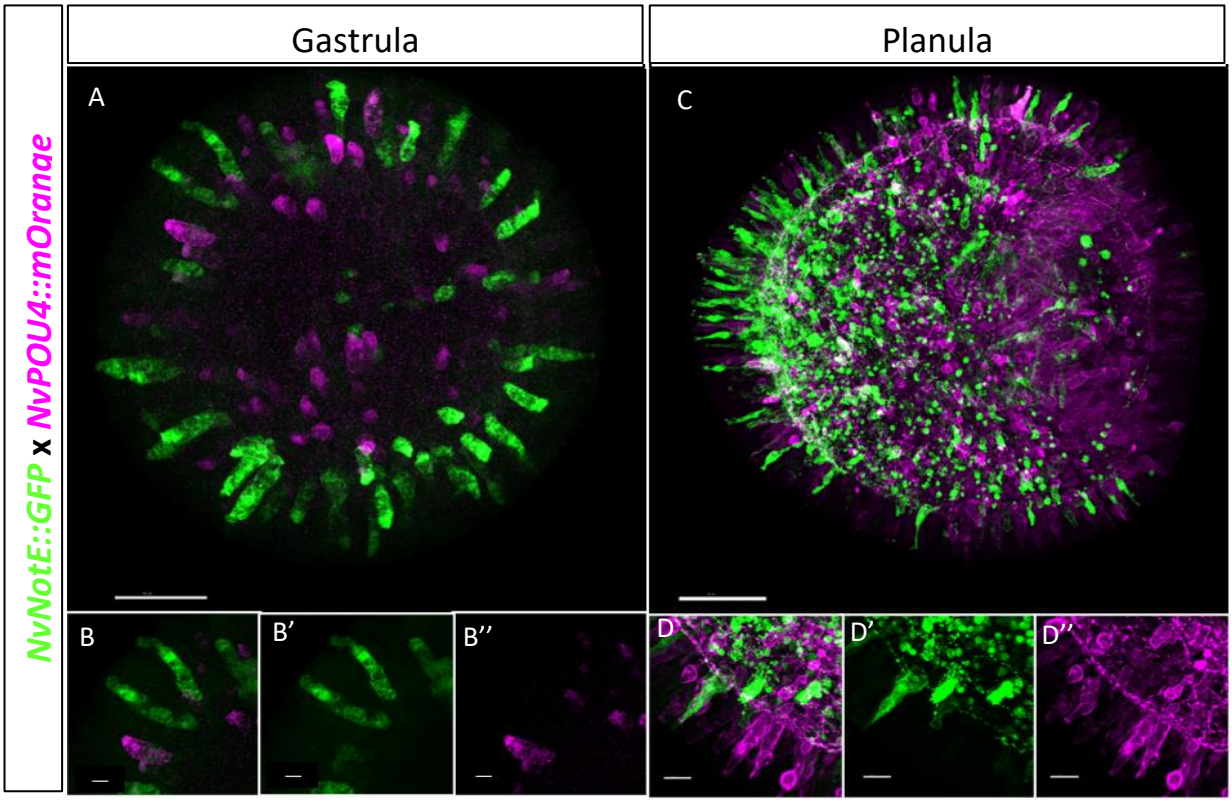

Figure 4.8.: *NvPOU4::mOrange* and *NvNotE::GFP* are not co-expressed. Double transgenic animals with *NvNotE*::GFP (green) crossed with *NvPOU4*::mOrange (magenta) reporter line labeling cnidocytes, sensory and ganglion cells. Transgenes are indicated to the left and developmental stages on top. Animals are oriented with their oral pole to the right. No co-expression between *NvNotE*::GFP and *NvPOU4*::mOrange was observed at gastrula stage (20hpf), or planula stage (72hpf) (A-D''). White color in (C) is due to the 3D reconstruction and does not represent co-expression. All images are 3D reconstructions. Scale bars: 50 µm (A, C), 10 µm (B, D).

4.2.4 *NvNotE::*GFP *expressing cells* do not appear to co-express *NvElav1* transgene

NvElav1::mOrange is a neuron-specific reporter line, labelling a subset of sensory and ganglion cells, but not cnidocytes (Nakanishi et al., 2012). As *NvNotE* was found to not be co-expressing

with cnidocyte marker *NvNcol3* (Figure 4.5 E), nor *NvPOU4::mOrange* reporter line, it was interesting to investigate if *NvNotE*-transgene expressing cells were a subset of *NvElav1* transgenes labelled cells. Double transgenic animals do not show cells co-expressing the *NvNotE* and *NvElav1* transgenes at planula and late planula stage (Figure 4.9 A-D'').

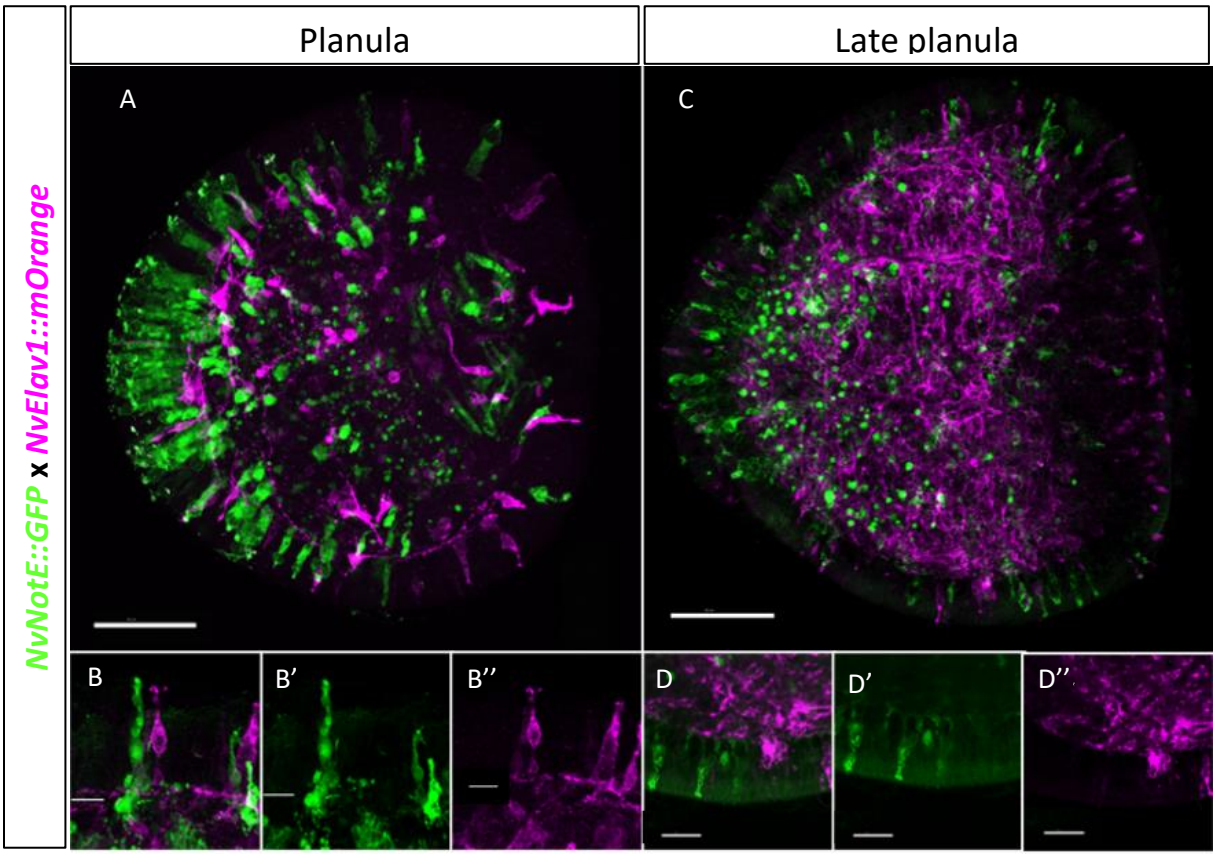

Figure 4.9: Some *NvNotE*::GFP expressing cells express *NvElav1* transgene later in development. Double transgenic animals with *NvNotE*::GFP (green) crossed with *NvElav1*::mOrange (magenta) reporter line labeling a subset of sensory and ganglion cells. Transgenes are indicated to the left. Developmental stages are shown on the top. Animals are oriented with their oral pole to the right. At planula (72hpf) and late planula (96hpf) cells expressing both transgenes are not observed (A-D''). At primary polyp (7dpf), few cells expressing the *NvNotE* transgene also appear to express the *NvElav1* transgene (E-F''). All images are 3D reconstructions. Scale bars: 50 µm (A, C, E), 10 µM (B, D, F)

4.2.5 Most *NvNotE*::GFP expressing cells do not express the *NvFoxQ2d::mOrange* transgene

The *NvFoxQ2d::mOrange* reporter line labels a subtype of sensory cells (Busengdal & Rentzsch, 2017). DFISH did not reveal co-expression between *NvFoxQ2d* and *NvNotE* (figure 4.5 H), but they might be expressed sequentially in the same cells, and it is therefore interesting to investigate if

they share progeny cells. To do this, double transgenic animals were generated by crossing *NvFoxQ2d*::*mOrange* to *NvNotE*::*GFP*. At planula stage, few cells expressing GFP also expressed the *NvFoxQ2d* transgene (Figure 4.10 A-B''). At primary polyp, no co-expression between the *NvNotE* transgene and *NvFoxQ2d* transgene is observed (Figure 4.10 C-D'').

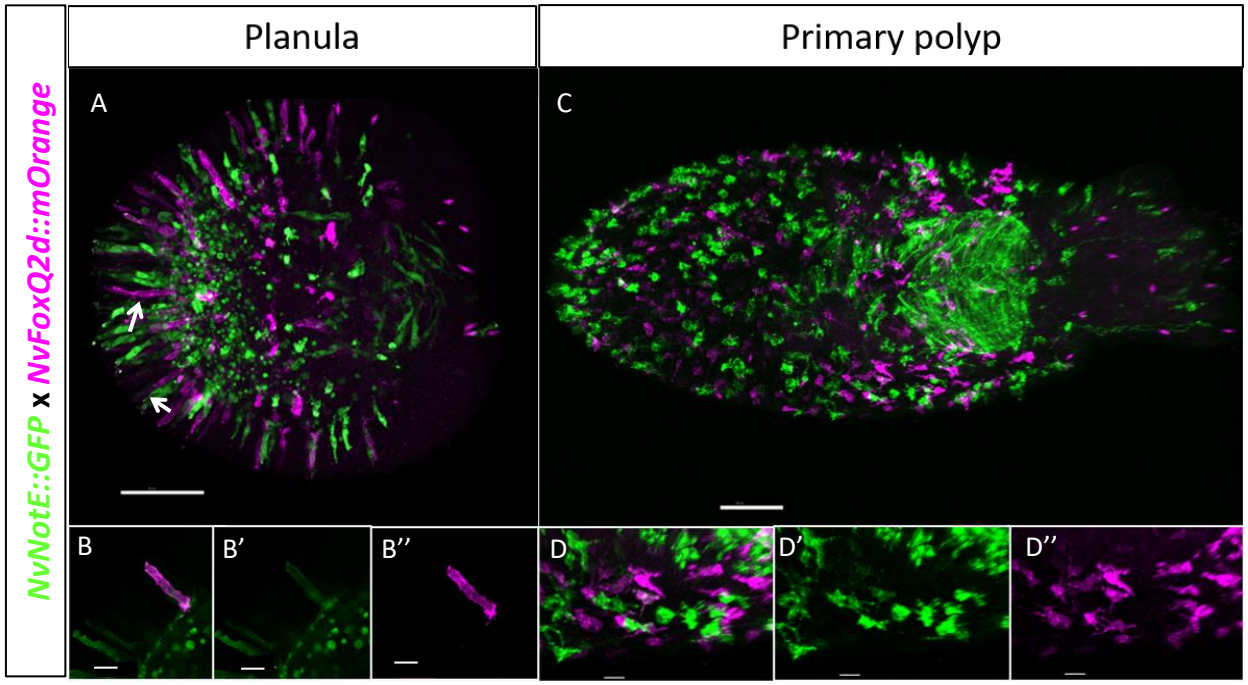

Figure 4.10: Almost no *NvNotE*::GFP-expressing cells also express the *NvFoxQ2d* transgene. Double transgenic animals with *NvNotE*::GFP (green) crossed with *NvFoxQ2d*::mOrange (magenta) reporter line labeling a subtype of sensory cells. Transgenes are indicated to the left. Developmental stages are shown on the top. Animals are oriented with their oral pole to the right. At planula stage (72hpf), a small number of cells expressing *NvFoxQ2d* transgene also express the *NvNotE* transgene (A-B''). At primary polyp stage (7dpf), no co-expression is observed (C-D''). (A, C, D) are 3D reconstructions, (B) is single confocal slice. Scale bars: 50 µm (A, C), 10 µm (B, D).

4.2.6 *NvNotE* and *NvInsm1* transgenic reporter line shows partially overlapping expression early in development

DFISH revealed that *NvInsm1* is co-expressed with *NvNotE* at gastrula stage, early planula stage, and at planula stage (Figure 4.4 M-R''). To investigate the relationship between *NvInsm1* and *NvNotE* further, double transgenic animals were generated by crossing *NvNotE::GFP* to *NvInsm1*::*mCherry* reporter line recently shown to label neurons and secretory cells (Tournière et al., 2021). At gastrula stage, there is co-expression between GFP and mCherry (Figure 4.11 A-B''). Notably the co-expression is not absolute as there are more cells expressing the *NvInsm1*

transgene than cells expressing *NvNotE* transgene. Most *NvNotE*::GFP-expressing cells appear to express *NvInsm1::*mCherry. However later in development, at planula and primary polyp stage, co-expression between *NvInsm1* transgene and *NvNotE* transgene is no longer observed (Figure 4.11 C-F'').

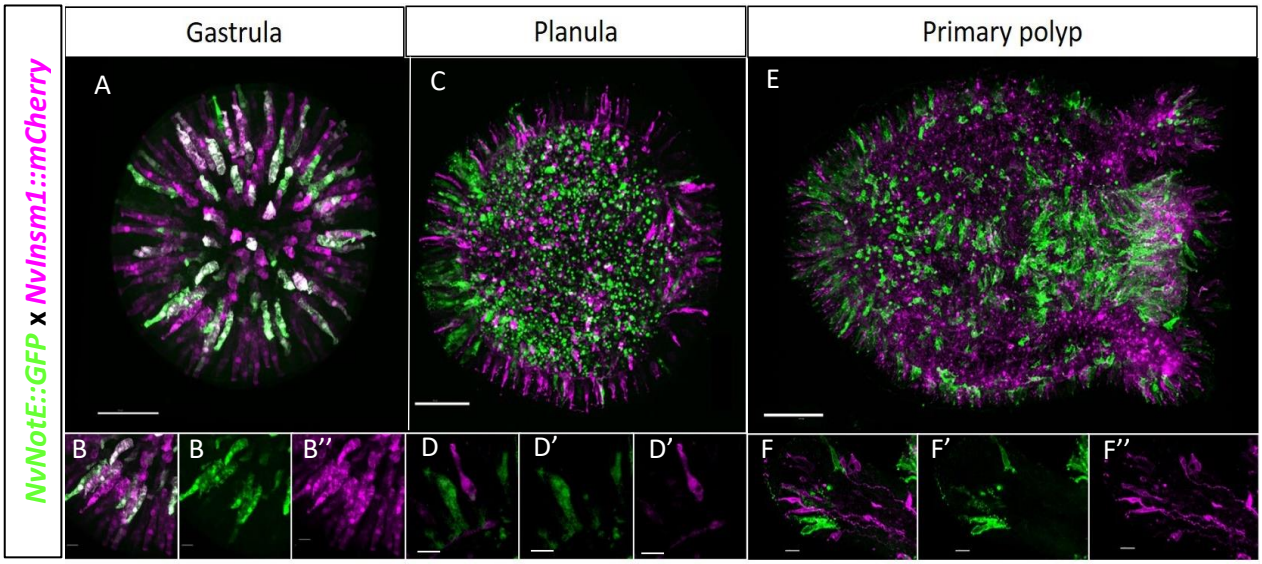

Figure 4.11: *NvNotE*::GFP-expressing cells is co-expressed with the *NvInsm1* transgene. Double transgenic animals with *NvNotE*::GFP (green) crossed with *NvInsm1*::mCherry (magenta) reporter line labeling neurons and secretory cells. Transgenes are indicated to the left and developmental stages shown on top. Animals are oriented with their oral pole to the right. At gastrula stage (20hpf), the majority of *NvNotE*::GFP-expressing cells are also expressing the *NvInsm1* transgene (A-B''). Though, there are several cells exclusively expressing the *NvInsm1* transgene (A-B''). At planula (72hpf) and primary polyp stage (7dpf), co-expression between *NvNotE* transgene and the *NvInsm1* transgene is not observed (C-F''). (A, B, C, E) are 3D reconstructions, (D, F) are single confocal slices. Scale bars: 50

Taken together, *NvNotE::*GFP-expressing cells are co-labelled with the progenitor marker *NvSoxB(2)* transgene early in development. *NvNotE::*GFP cells are also found to be co-labeled with *NvInsm1* transgene at early gastrula, meanwhile no co-labelling with *NvPOU4* transgene was found. In addition, co-labelling with the sensory cell marker *NvFoxQ2d* and *NvElav1* was not found at planula and primary polyp stage, respectively. In summary this suggests that the *NvNotE* cells mainly give rise to gland/secretory cells and likely to a small number of sensory cells.

4.3 CRISPR/Cas9 strategy is successful in creating *NvNotE* mutants

Now that the *NvNotE* expressing cells and their progeny have been characterized, it was interesting to study the function *NvNotE*. To do this, fertilized eggs were injected with sgRNAs and the Cas9 protein to generate a mutant line (Section 3.7). The *NvNotE* gene is a small gene

(1685 bp), consisting of a 367 bp first exon and a second 278 bp exon containing the homeobox domain (HD), separated by a 367 bp intron (Figure 4.12).

4.3.1 CRISPR/Cas9 mediated mutagenesis cause premature stop codon in *NvNotE*

Three single guide RNAs (sgRNA1, sgRNA2 and SgRNA3) were designed to target the beginning of exon 1 (Table 2.1.3, Figure 4.12). The goal is to introduce an indel mutation that will generate a frameshift and an early stop codon. Injected animals were grown to primary polyp stage before genomic DNA was extracted (Section 3.7.).

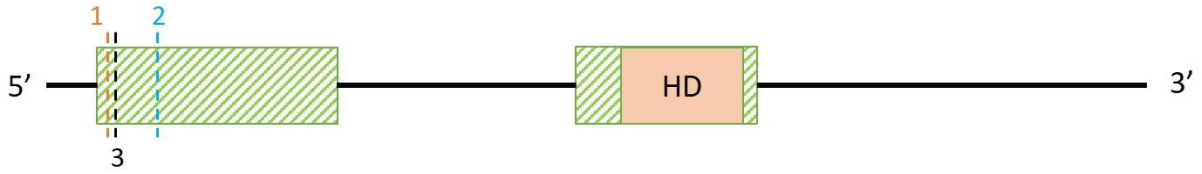

Figure 4.12: Schematic of CRISPR/Cas9 genome editing strategy for *NvNotE*. The *NvNotE* gene consists of 1685 bp with two exons of 367 bp and 278 bp. The second exon contains a conserved homeobox domain (HD) shown in orange. Three single guide RNAs, sgRNA1 (orange), sgRNA2 (blue), sgRNA3 (black) were designed to target the start of exon 1. The schematic is to scale.

To evaluate the success of the sgRNAs in introducing mutations, EvaGreen melt curves were performed with the extracted genomic DNA (Section 3.8). EvaGreen only emits fluorescence when bound to double stranded DNA. The thermal cycler gradually increases the temperature whilst detecting fluorescence. When DNA denatures, the EvaGreen will dissociate. This is a quick process without an intermediate state and can be visualized as a melting curve. The derivative melting curve describes the change of the slope, with the peak corresponding to the maximum change of the slope, in other words, the melting point. The melting temperature is sequence specific, meaning that a change in the sequence, for example caused by an indel mutation, will alter the slope.

For control, melt curve analysis of non-injected animals from the same batch was performed with the corresponding primer pairs (Table 2.1.3). Eight control animals were tested for each primer pair, a representative is shown in red, while injected animals are shown in blue (Figure 4.13). The majority of the melt curves of sgRNA1-injected animals (6/7) have a “shoulder”

compared to the control animals indicating the presence of a mutation (Figure 4.13 A). This is also observed for sgRNA2 injected animals, where 7/8 animals tested show a shift in their slope compared to the control (Figure 4.13 B). For animals injected with sgRNA3, 8/8 of the animals tested appear to contain a mutation indicated by the presence of a "shoulder" (Figure 4.13 C). This suggests that the CRISPR/Cas9 system was successful in causing alterations in the sequence for all sgRNAs injected.

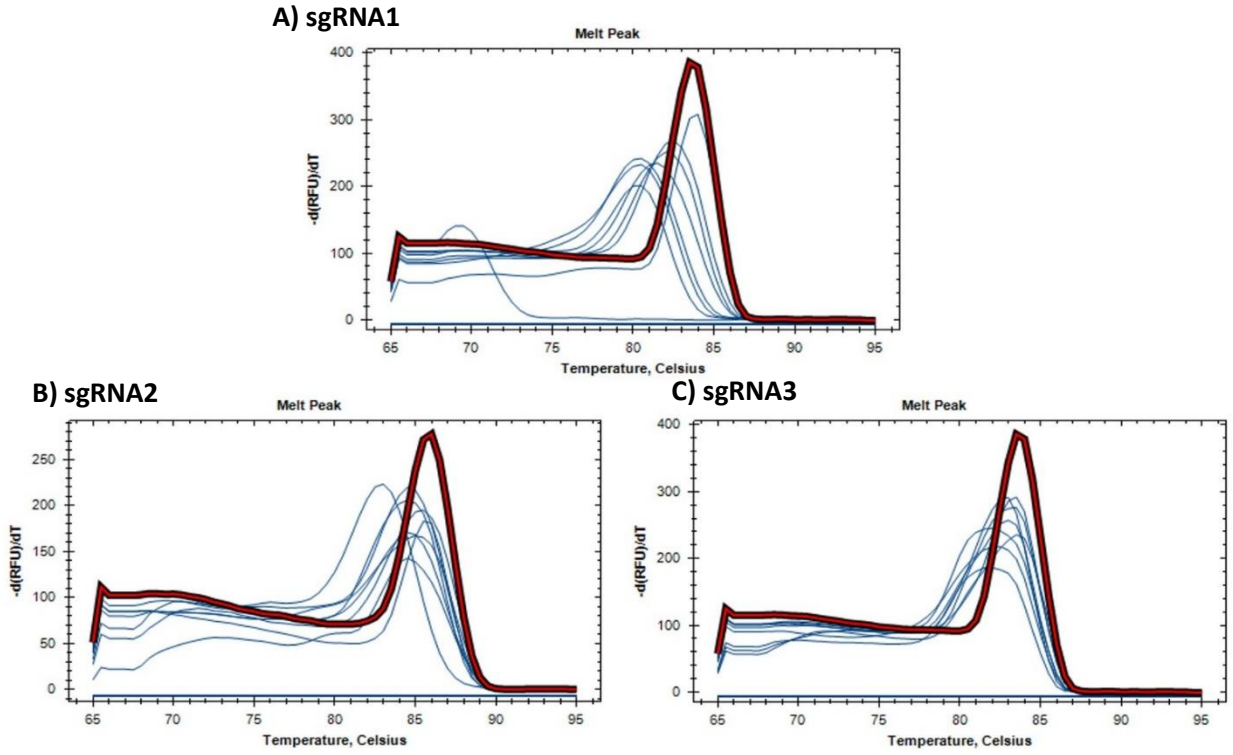

Figure 4.13: CRISPR/Cas9 system successfully introduced mutations in *NvNotE*. Three single guide RNAs (sgRNA) were designed to target the start of exon 1 in NvNotE sequence. Genomic DNA was extracted from sgRNA injected animals at polyp stage and analyzed by EvaGreen melt curve. Alterations to the sequence causes a change in the melting temperature indicated by a shift in slope. Eight wild type animals were tested, a representative is shown in red. Injected animals are shown in blue. X-axis show the temperature (°C), the Y-axis show the change of fluorescence [-d(RFU)] per unit change in temperature (dT). 6/7 of SgRNA1-injected animals show a shift in the melting curve indicating a mutation in the sequence (A). 7/8 sgRNA2-injected animals (B), and 8/8 sgRNA3-injected animals (C) appears to have an altered sequence indicated by the presence of a "shoulder" compared to the control animals.

As all three of the sgRNAs appear to introduce changes in the DNA sequence, the injected animals were grown to sexual maturity before they were crossed to wild type. F0 carriers were identified by melt curve analysis of genomic extraction of whole F1 animals as described above. Melt curves fail to disclose the nature of the mutation, so genomic DNA of F1 animals suspected to carry

mutations were sent to sequencing. No possible carriers were identified for sgRNA1-injected animals. For one sgRNA2-injected animal, genotyping of F1 animals revealed a 7 bp insertion in all four animals sent for sequencing, causing a frameshift that leads to a premature stop codon 269 bp into exon 1 (Figure 4.14).

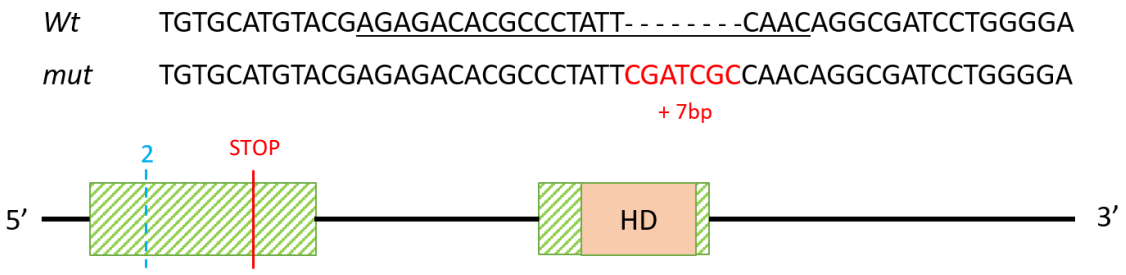

Figure 4.14: sgRNA2 injection generates a 7 bp insertion causing a premature stop codon. F0 carriers were identified by melt curve analysis and sequencing of F1 animals. Genotyping of F1 animals of sgRNA2-injected F0 founder, revealed a 7 bp insertion leading to a frame shift, causing a premature stop codon 269 bp into exon 1 (indicated by red line).

For one sgRNA3-injected animals genotyping of F1 animals revealed a 5 bp deletion and a 2 bp substitution for two animals sent to sequencing, causing a frameshift leading to the same premature stop codon as for sgRNA2-injected animals, 269 bp into exon 1 (Figure 4.15).

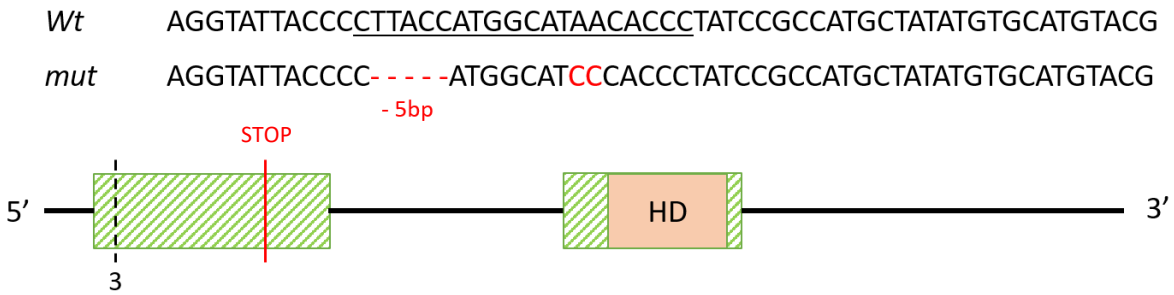

Figure 4.15: SgRNA3 injection causes a 5 bp deletion resulting in a premature stop codon. F0 carriers were identified by melt curve analysis and sequencing of F1 animals. Genotyping of F1 animals of sgRNA3-injected F0 founder, revealed a 5 bp deletion and a 2 bp substitution leading to a frame shift, consequently generating a premature stop codon 269 bp into exon 1 (indicated by red line).

Taken together, two founders that induce frameshift mutation in F1 offspring were identified. Next the F1 of these founders will be grown to a size where the foot can be cut off for genotyping

to identify F1 animals carrying frameshift mutations. Heterozygous mutants will subsequently be in-crossed to generate homozygous mutants.

4.3.2. Double injection of sgRNA cause excision of the *NvNotE* coding sequence

To be sure that the mutation was significant enough to eliminate *NvNotE* gene function, a double injection of sgRNA was done with the goal of excising the coding sequence. Based on frequency of mutation observed in injected animals by melt curve, sgRNA3 was selected to target the start of exon 1 (Figure 4.13). Three sgRNAs were designed to target the 3' UTR of the gene. The co-injected animals were grown to polyp stage, PCR was used to amplify the target region, and checked by agarose gel to look for mutants (Section 3.7). 5/7 of the tested animals injected with sgRNA3 and sgRNA6 showed a band corresponding to the expected size (approx. 375bp) with the gene excised (Figure 4.16 B). SgRNA3 + sgRNA6-injected animals were grown to sexual maturation and crossed to wild type to identify an F0 carrier. PCR of pooled genomic DNA extracted from F1 followed by 1% agarose gel electrophorese identified a F0 carrier of the deletion mutation (Figure 4.16 C).

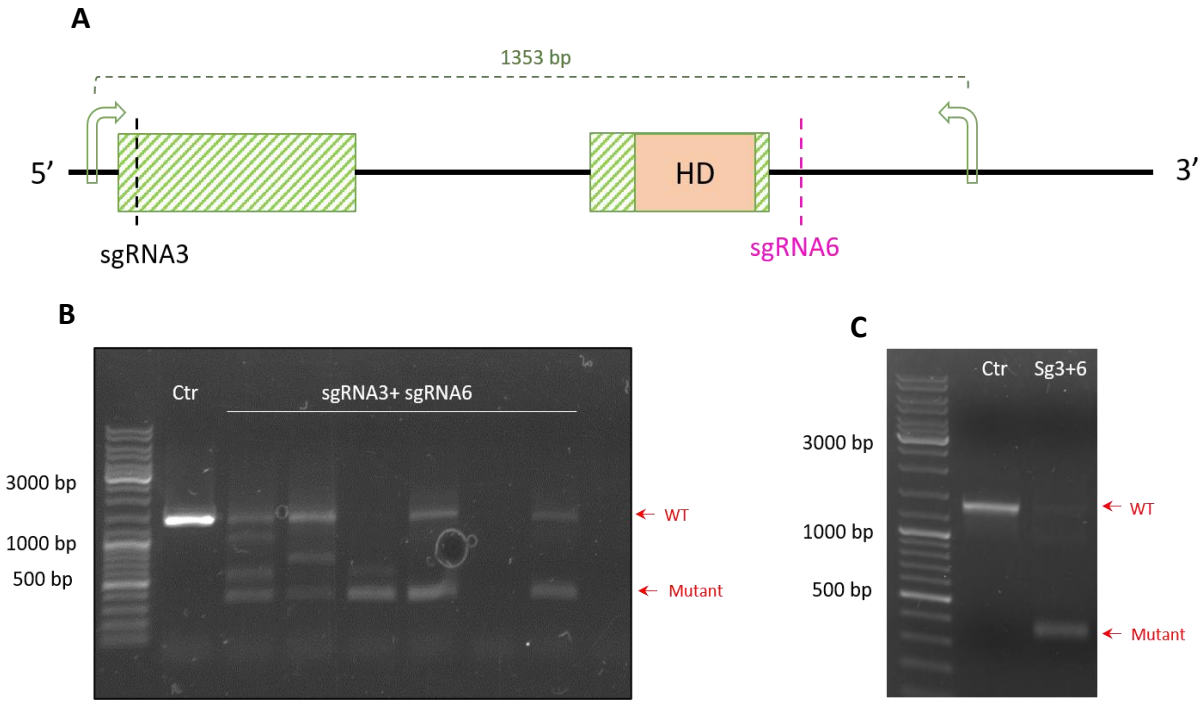

Figure 4.16: Co-injection of sgRNA3 and sgRNA6 successfully excises the coding region of *NvNotE*. To excise the coding region of *NvNotE*, fertilized animals were co-injected with sgRNA3 and sgRNA6 targeting the start of exon 1 and the 3' UTR region, respectively (Figure 4.16., A). Arrows indicates forward and reverse PCR primers amplifying a 1353 bp region in wild type (A). 1% agarose gel electrophorese show genomic DNA of five co-injected animals with a band corresponding to the *NvNotE* sequence without the coding sequence at approx. 375 bp (B). SgRNA3 + SgRNA6-injected animals were grown to sexual maturation and crossed to wild type. Genotyping of F1 animals identified a F0 carrier of the deletion mutation (C). Sg3+sg6 indicates a pool of genomic DNA from eight F1 animals from a F0 co-injected founder (C).

To summarize, the CRISPR/Cas9 strategy was successful in creating mutant animals, both with indel mutations causing premature stop codon and to excise the coding sequence of the *NvNotE* gene.

5. Discussion

To be able to compare the development of neurons to gland/secretory cells, it is beneficial to gain a better understanding of how gland/secretory cells are specified across species. Here we use *Nematostella* as a model for early branching animals in order to address this. A diverse array of gland/secretory cells have been identified in *Nematostella*, however developmental genes that act specifically in specifying gland/secretory cells remain enigmatic. This study aimed to investigate the role of *Not* homeobox genes in *Nematostella*, and thereby be able to understand how gland/secretory cells are specified. ISH revealed that *NvNotA*, *NvNotC* and *NvNotE* are expressed in scattered cells during development. Furthermore, *NvNotE* was shown to be co-expressed with known gland/secretory markers. Finally, CRISPR/Cas9 was successfully used to generate *NvNotE* mutants which will facilitate future studies on the function of *NvNotE*.

5.1 *NvNotA*, *NvNotC* and *NvNotE* are expressed in scattered cells.

The homeobox genes *NvNotA, NvNotC* and *NvNotE* were identified to have a possible role in neurogenesis by a microarray screen to identify neural genes. All three *NvNot* genes were found to be expressed in scattered cells. *NvNotA* is expressed only in the mesendoderm from planula stage, while *NvNotC* is found in both the ectoderm from gastrula stage and later in the mesendoderm. *NvNotE*-expression is initiated early, and expression is only observed in the ectoderm (Figure 4.1, Figure 4.2). DFISH of *NvNotE* with *NvNotC* and *NvNotA* does not show any co-expression (Figure 4.5). However, a more detailed time course would help establish if the cells in the aboral ectoderm, shown for both *NvNotC* and *NvNotE*, are the same. Furthermore, we do not know if the cells expressing *NvNotA* and *NvNotC* in mesendoderm are the same cells, which would be interesting to investigate with DFISH. Little is known about the nature of these cells. Generating stable transgenic lines for *NvNotA* and *NvNotC* would allow us to get a better understanding of their morphology, as well as to investigate what they develop into.

The *Not* homeobox genes have been duplicated in the lineage leading to *Nematostella* (Chourrout et al., 2006). With a duplication it is difficult to elucidate the ancestral function, as the genes might have undergone a subfunctionalization, where each gene copy only keep parts of the function, but together make up the ancestral function, or neofunctionalization where one

copy retains the ancestral function while the other gene copies gain new functions (Assis & Bachtrog, 2013). To gain further insight into the ancestral role of *Not* homeobox genes, *Not* paralogs in *Nematostella* need to be studied further as well as compared to orthologous in other species, for example in *Hydra*, which only contain one *Not* homeobox gene like in bilaterians (Gauchat et al., 2000).

5.2 *NvNotE* is expressed in *NvMucin* expressing gland/secretory cells.

The expression pattern for *NvNotE* resembles that of a known gland/secretory cell marker, *NvMucin* (Figure 4.2 A-L), with expression in the ectoderm and later in the pharynx (Figure 4.2 M-X). Interestingly, only a very weak expression was observed for *NvMucin* at blastula stage. This may suggest that *NvMucin* expression is initiated later than *NvNotE,* or it could be due to technical limitations. Furthermore, it appears more cells express *NvMucin* than *NvNotE*. Co-expression between the two genes reveals that almost all cells expressing *NvNotE* also express *NvMucin* (Figure 4.4). This strongly suggest that *NvNotE* is expressed in a subset of *NvMucin*-expressing gland/secretory cells in *Nematostella*. This was further validated by a single cell atlas of *Nematostella* showing that *NvNotE* is expressed in *NvMucin* gland cells (Sebé-Pedrós et al., 2018).

To address whether the lack of an absolute co-expression between *NvMucin* and *NvNotE* is due to temporal differences in expression, DFISH in the background of *NvNotE*::GFP transgenic reporter line would reveal if all GFP positive cells also express *NvMucin*. This protocol was recently developed and performed for *NvInsm1*::GFP with gland/secretory markers (Tournière et al., 2021). For *NvNotE*, this would allow us to better characterize the identity of *NvNotE*-expressing cells and the nature of a possible population of putative specific gland/secretory cells that they contribute to. In addition, looking at how *NvMucin* cells are affected in *NvNotE* mutants would allow us to understand the relationship between *NvNotE*-expressing and *NvMucin*-expressing cells better. If *NvNotE* is required for the expression of *NvMucin* and all *NvMucin*-expressing cells express *NvNotE*, we would expect to see no *NvMucin*-expressing cells.

The morphology of the *NvNotE* cells was investigated by transgenic reporter line, and cells expressing *NvNotE*::GFP were found in the ectoderm at the aboral pole earlier in development before expression of the transcript can be found in the ectodermal body column, pharynx and in the tips of the tentacles (Figure 4.6). Some of the cells expressing the *NvNotE* transgene, were observed to have an apical cilium and basal processes. By DFISH we known that almost all *NvNotE* ectodermal cells are *NvMucin*$^{+}$, and therefore this presents evidence of gland/secretory cells in *Nematostella* having processes. Non-neural cells with processes have been observed in muscle cells in the nematode *Caenorhabditis elegans* (Kristan, 2016) and also in entero-endocrine cells in vertebrates (Hartenstein et al., 2017).

The elongated shape of the cells found in the tentacle tips and pharynx compared to the more roundish appearing cells in the body column may indicate different cell types, however, this is most likely due to "stretching" of the ectodermal tissue in the tentacles compared to the body column. Additionally, cells spanning the ectoderm at gastrula stage are observed with vesicle-like structures compatible with a gland/secretory cell identity. No reporter line was available for *NvMucin*, but ISH revealed expression in the tentacles for *NvMucin* as well as in the pharynx and ectodermal body column at primary polyp stage (Figure 4.2). DFISH with *NvMucin* and *NvNotE* at primary polyp stage, would address if these are the same cells. This study shows *NvNotE* as an ectodermally expressed gene, however expression of *NvMucin* have also been observed in the mesendoderm of the body wall (Steinmetz et al., 2017). From results presented here, we cannot exclude expression of *NvNotE* in the mesendodermal part of the mesenteries. ISH of cross sections with high magnification of the mesenteries could help to assess the potential expression of *NvNotE* in the mesenteries.

5.3 A role for *NvNotE* in neurogenesis in *Nematostella* is ambiguous.

Neuropeptides *NvLWamide* and *NvRFamide* are not found to be co-expressed with *NvNotE* (Figure 4.5 F, G), and no co-expression is observed with transgenes of other neuronal markers like *NvPOU4* and *NvElav1* (Figure 4.8, Figure 4.9). Results from this study also show no co-expression with *NvNcol3*, suggesting that *NvNotE* is not expressed in cnidocytes (Figure 4.5. E). A small number of *NvFoxQ2d*-transgene expressing cells were however shown to express the

NvNotE transgene. This was not observed by DFISH, leaving the relationship between *NvNotE* and *NvFoxQ2d* (expressed in a small population of sensory neurons) ambiguous. As the transgene is detectable in the cell after expression is terminated, an explanation could be that *NvFoxQ2d* expression is ceased before *NvNotE* is expressed sequentially in the same cells. The results from this study does not allow a conclusion to this question.

5.2 *NvNotE* is expressed in a subpopulation of *NvInsm1*-expressing cells.

A recent study confirmed that gland/secretory cells originates from a common pool of *NvSoxB(2)* positive progenitor cells, previously thought to just give rise to neural cells (Tournière et al., 2021). The study showed that *NvInsm1* is expressed in a subset of *NvSoxB(2)*$^{+}$ progenitors that give rise to sensory neurons and gland/secretory cells, including *NvMucin*$^{+}$ cells (Tournière et al., 2021). *NvFoxQ2d* is known to be expressed in cells giving rise to a group of sensory cells. In addition, all *NvFoxQ2d* cells are found to derive from *NvInsm1* cells, as well as expressing *NvInsm1*.

This prompted us to investigate if *NvNotE*$^{+}$ cells originate from *NvSoxB(2)*$^{+}$ progenitor cells. Indeed, *NvNotE* and *NvSoxB(2)* are co-expressed early in development, however there are more cells that only express one of the transcripts (Figure 4.4 A-E, Figure 4.7). There are two, not mutually exclusive, alternative explanations for this. There might be a *NvNotE-expressing* cell population that is not derived from the *NvSoxB(2)* expressing population, or it might be due to temporal differences in the expression of *NvSoxB(2)* and *NvNotE*. The *NvSoxB(2)* pool of progenitors includes cells that are proliferating (Richards & Rentzsch, 2014), though no EdU incorporation was shown for *NvNotE* cells after 30 min labelling (Figure 4.3). This could mean that expression of *NvNotE* is initiated in cells that have stopped proliferating but are still expressing *NvSoxB(2). In situ* hybridization for *NvNotE* in *NvSoxB(2)* mutants would aid in understanding the relationship between *NvNotE* and *NvSoxB(2)*, in addition to further EdU experiments.

Expression of *NvInsm1* starts at blastula stage (Tournière et al., 2021), similar to *NvNotE*. *NvNotE* and *NvInsm1* were also found to be expressed in the same cells, although with more cells only expressing *NvInsm1* (Figure 4.4 M-Q). There is some discrepancy between the DFISH and

transgenic crosses. As DFISH shows co-expression later in development, although in few cells, it would be anticipated that co-expression of the two transgenes would be observed at later time points (Figure 4.11). However, we do not see co-expression of the transgenes at planula stages. The absence of this could be due to the transgenic line not completely reflecting the endogenous expression of *NvNotE*. Though, a pattern is observed in both the transgenic crosses and with DFISH, of early co-expression, which is later gone or minimized between *NvNotE* and *NvInsm1*. Possible explanations for this are that the *NvNotE*::GFP transgene being diluted through series of cell divisions, or that cells expressing *NvNotE::*GFP early in development undergo apoptosis and expression is initiated later in development in an unrelated group of cells. As EdU labelling found *NvNotE*-expressing cells to not be proliferating, the former possibility is deemed unlikely. TUNEL assay in *NvNotE*::GFP animals would reveal if the cells undergo apoptosis and would allow to trace the potentially dying cells.

Most *NvNotE* expressing cells do not express *NvFoxQ2d,* nor derive from *NvFoxQ2d*-expressing cells (Figure 4.5 H, Figure 4.10). This may suggest that *NvFoxQ2d* is expressed in a subpopulation of *NvInsm1* cells that will later develop into sensory neural cells while *NvNotE* is expressed in a subpopulation of *NvInsm1*-expressing cells developing into gland/secretory cells. Notably, gland/secretory markers *NvTrypsinA* and *NvIlp2* are co-expressed with *NvInsm1* (Tournière et al., 2021), but not with *NvNotE* (Figure 4.5 C, D). This indicates that *NvNotE* is expressed in a specific gland/secretory subgroup later in development that is not labelled by *NvTrypsinA* and *NvIlp2.*

The cell differentiation trajectory of neurons and gland/secretory cells in *Nematostella* is still enigmatic. This study proposes a hypothesis for the specification of a subpopulation of gland/secretory cells in *Nematostella* (Figure 5.1). In this proposal, a group of *NvSoxB(2)*-expressing progenitor cells gives rise to at least two groups of cells, where one group gives rise to cnidocytes, while another group of cells is characterized by expression of *NvInsm1*. The *NvInsm1* expressing group would then give rise to a pool of *NvInsm1* and *NvFoxQ2d*-expressing cells that would give rise to a subset of sensory neurons. The other group of *NvInsm1*$^{+}$ cells would give rise to *NvInsm1* expressing gland/secretory cells where one subgroup express *NvMucin* and *NvNotE,* and another *NvTrypsinA* and *NvIlp2.* Another alternative is that an initially homogeneous group of *NvSoxB(2)*-expressing progenitor cells becomes a heterogenous pool of linage restricted

progenitors, where *NvInsm1* is expressed in an unrelated fashion in different progenitor groups, that individually give rise to cnidocytes, sensory and ganglion neurons and to gland/secretory cells, one being the *NvNotE-expressing* cells. To test the different hypothesis, generating a photoconvertible fluorescent *NvInsm1* transgenic line, would allow us to track individual cells

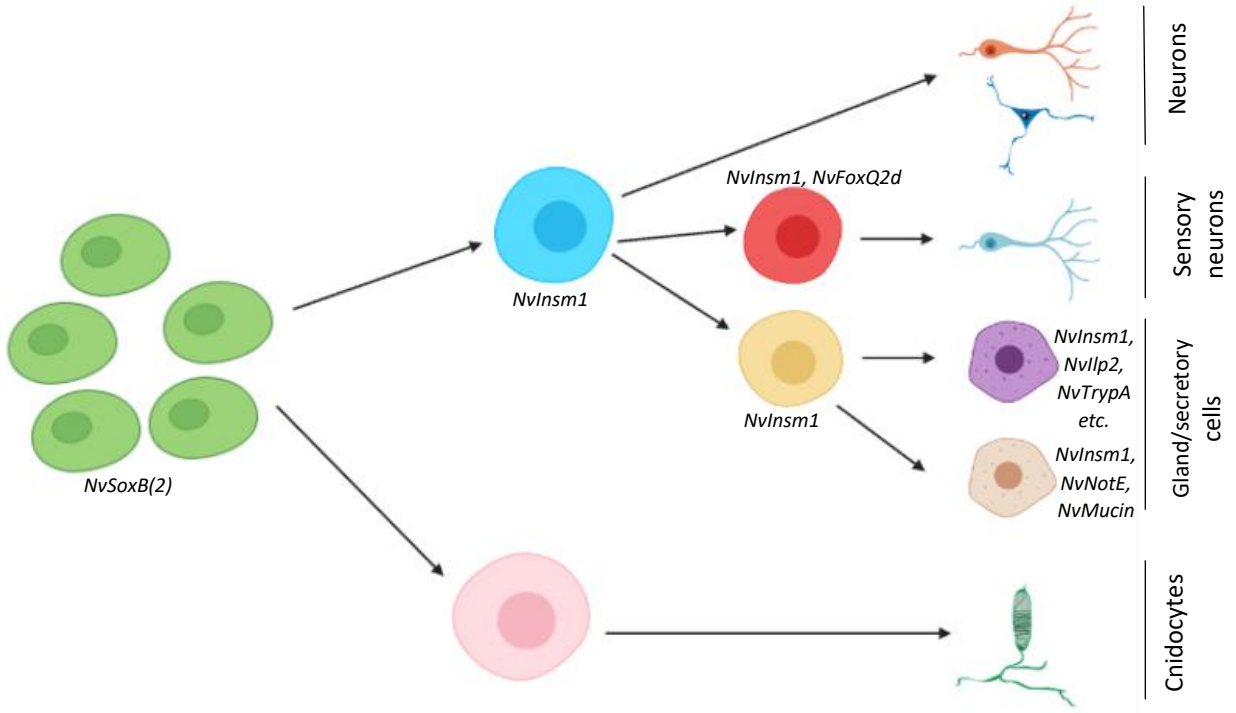

Figure 5.1: Possible cell differentiation trajectory in *Nematostella*. A pool of *NvSoxB(2)*-expressing progenitor cells give rise to more restricted pool of cells. The *NvInsm1*-expressing group of cells give rise to *NvInsm1*-expressig group of cells where one group also express *NvFoxQ2d*. The *NvFoxQ2d*-expressing cells would then give rise to a group of sensory neurons, while the other group would give rise to *NvMucin* expressing gland/secretory cells also expressing *NvNotE*. Figure created in BioRender.com and modified from Océane Tournière

5.4 CRISPR/Cas9 was successful in creating mutant *NvNotE*-animals.

To gain insight into the function of *NvNotE*-expressing cells, CRISPR/Cas9 was used to generate *NvNotE* mutants with a premature stop codon (Figure 4.14, Figure 4.15), or the coding sequence excised (Figure 4.16). *NvNotE* mutants have been crossed to *NvElav1*::mOrange, *NvFoxQ2d*::mOrange, *NvNotE*::GFP and *NvInsm1*::GFP. They are yet to be examined but will allow us to analyze the mutants in the background of the transgenics.

To be able to characterize the functional role of *NvNotE*, homozygous animals must be generated by in-crossing of heterozygous F1 animals. Due to the generation time of *Nematostella*, this was not possible within the given timeline. For further studies, *in situ* hybridization for different cell markers in homozygous mutant *NvNotE* animals would help to give insight into its functional role.

As well as the mutant crosses with transgenic reporter lines. Visual examination could also reveal if mutation in *NvNotE* leads to a specific morphological or gross behavioral phenotype. Expression of *NvMucin* has been found to be upregulated during wound healing in *Nematostella* (DuBuc et al., 2014). A similar function is observed in mice where it is involved in wound healing in the gastric mucosa (Ikezawa et al., 2004). If *NvNotE* mutants have deficiencies in the development of *NvMucin*-expressing cells, investigating whether the mutant animals have regenerative or wound healing defects would give insight into the functional role of these gland/secretory cells.

5.5. Conclusion and further perspectives.

With this study we wanted to investigate how gland/secretory cells are specified and differentiated in *Nematostella*. Result shown here reveal that *NvNotE* is expressed in *NvMucin*-expressing gland/secretory cells and appears to be the first transcription factor identified to be expressed specifically in gland/secretory cells. *NvInsm1* acts as a broad regulator of neural and gland/secretory cells, while *NvNotE*-expression is more specific in a subpopulation of *NvInsm1* and *NvMucin* expressing gland/secretory cells. However, we do not know if *NvNotE* is required for the differentiation of these cells. We are left with no clear answer to the evolutionary role of *Not* genes. In *Nematostella, Not* genes appear to act in the development of cell types, unlike what is shown for bilaterians where it acts in a broader region or tissue. Furthermore, published expression patterns of *Not* genes in bilaterians are described in neural structures and *Not* genes have not yet been described in *Mucin* expressing cells.

To obtain a better understanding of cell type specification in *Nematostella*, RNA sequencing of the whole transcriptome of homozygous *NvNotE* mutant, would allow us to identify genes downstream of *NvNotE*. Identifying more transcription factors involved in the specification of gland/secretory cells would also elucidate how these cells are specified in *Nematostella*. To better investigate the relationship between *NvNotE* and *NvMucin*, a transgenic reporter line for *NvMucin* would allow to better understand the nature of the co-expression. In addition, generating a more detailed expression time course by DFISH, especially for *NvNotE* with *NvMucin* and *NvInsm1*, the latter to affirm when in development *NvInsm1* and *NvNotE* co-expression ceases.

6 References

Altenburger, A., Martinez, P., & Wanninger, A. (2011). Homeobox gene expression in Brachiopoda: The role of Not and Cdx in bodyplan patterning, neurogenesis, and germ layer specification. *Gene Expression Patterns*, *11*(7), 427-436. https://doi.org/https://doi.org/10.1016/j.gep.2011.07.001

Arendt, D. (2020). The Evolutionary Assembly of Neuronal Machinery. *Current Biology*, *30*(10), R603-R616. https://doi.org/https://doi.org/10.1016/j.cub.2020.04.008

Arendt, D., Bertucci, P. Y., Achim, K., & Musser, J. M. (2019). Evolution of neuronal types and families. *Current Opinion in Neurobiology*, *56*, 144-152. https://doi.org/https://doi.org/10.1016/j.conb.2019.01.022

Assis, R., & Bachtrog, D. (2013). Neofunctionalization of young duplicate genes in Drosophila. *Proceedings of the National Academy of Sciences*, *110*(43), 17409. https://doi.org/10.1073/pnas.1313759110

Babonis, L. S., & Martindale, M. Q. (2014). Old Cell, New Trick? Cnidocytes as a Model for the Evolution of Novelty. *Integrative and Comparative Biology*, *54*(4), 714-722. https://doi.org/10.1093/icb/icu027

Babonis, L. S., & Martindale, M. Q. (2017). PaxA, but not PaxC, is required for cnidocyte development in the sea anemone Nematostella vectensis. *Evodevo*, *8*(1), 14. https://doi.org/10.1186/s13227-017-0077-7

Babonis, L. S., Ryan, J. F., Enjolras, C., & Martindale, M. Q. (2019). Genomic analysis of the tryptome reveals molecular mechanisms of gland cell evolution. *Evodevo*, *10*, 23. https://doi.org/10.1186/s13227-019-0138-1

Beckers, A., Alten, L., Viebahn, C., Andre, P., & Gossler, A. (2007). The mouse homeobox gene Noto regulates node morphogenesis, notochordal ciliogenesis, and left–right patterning. *Proceedings of the National Academy of Sciences*, *104*(40), 15765. https://doi.org/10.1073/pnas.0704344104

Bertrand, N., Castro, D. S., & Guillemot, F. (2002). Proneural genes and the specification of neural cell types. *Nat Rev Neurosci*, *3*(7), 517-530. https://doi.org/10.1038/nrn874

Bode, H. R., Heimfeld, S., Chow, M. A., & Huang, L. W. (1987). Gland cells arise by differentiation from interstitial cells in Hydra attenuata. *Developmental Biology*, *122*(2), 577-585. https://doi.org/https://doi.org/10.1016/0012-1606(87)90321-6

Brunet, T., & Arendt, D. (2016). From damage response to action potentials: early evolution of neural and contractile modules in stem eukaryotes. *Philosophical transactions of the Royal Society of London. Series B, Biological sciences*, *371*(1685), 20150043. https://doi.org/10.1098/rstb.2015.0043

Bürglin, T. (2013). Homeobox Genes. In (pp. 503-508). https://doi.org/10.1016/B978-0-12-374984-0.00725-7

Burkhardt, P., & Sprecher, S. G. (2017). Evolutionary origin of synapses and neurons - Bridging the gap. *Bioessays*, *39*(10). https://doi.org/10.1002/bies.201700024

Burkhardt, P., Stegmann, C. M., Cooper, B., Kloepper, T. H., Imig, C., Varoqueaux, F., Wahl, M. C., & Fasshauer, D. (2011). Primordial neurosecretory apparatus identified in the choanoflagellate Monosiga brevicollis. *Proceedings of the National Academy of Sciences*, *108*(37), 15264-15269. https://doi.org/10.1073/pnas.1106189108

Bursztajn, S., & Davis, L. E. (1974). The role of the nervous system in regeneration, growth and cell differentiation in Hydra. *Cell and Tissue Research*, *150*(2), 213-229. https://doi.org/10.1007/BF00222171

Burton, P. M., & Finnerty, J. R. (2009). Conserved and novel gene expression between regeneration and asexual fission in Nematostella vectensis. *Development Genes and Evolution*, *219*(2), 79-87. https://doi.org/10.1007/s00427-009-0271-2

Busengdal, H., & Rentzsch, F. (2017). Unipotent progenitors contribute to the generation of sensory cell types in the nervous system of the cnidarian Nematostella vectensis. *Developmental Biology*, *431*(1), 59-68. https://doi.org/https://doi.org/10.1016/j.ydbio.2017.08.021

Campos-Ortega, J. A. (1995). Genetic mechanisms of early neurogenesis in Drosophila melanogaster. *Molecular Neurobiology*, *10*(2), 75-89. https://doi.org/10.1007/BF02740668

Chehrehasa, F., Meedeniya, A. C. B., Dwyer, P., Abrahamsen, G., & Mackay-Sim, A. (2009). EdU, a new thymidine analogue for labelling proliferating cells in the nervous system. *Journal of Neuroscience Methods*, *177*(1), 122-130. https://doi.org/https://doi.org/10.1016/j.jneumeth.2008.10.006

Chourrout, D., Delsuc, F., Chourrout, P., Edvardsen, R. B., Rentzsch, F., Renfer, E., Jensen, M. F., Zhu, B., de Jong, P., Steele, R. E., & Technau, U. (2006). Minimal ProtoHox cluster inferred from bilaterian and cnidarian Hox complements. *Nature*, *442*(7103), 684-687. https://doi.org/10.1038/nature04863

Darling, J. A., Reitzel, A. R., Burton, P. M., Mazza, M. E., Ryan, J. F., Sullivan, J. C., & Finnerty, J. R. (2005). Rising starlet: the starlet sea anemone, Nematostella vectensis. *Bioessays*, *27*(2), 211-221. https://doi.org/10.1002/bies.20181

David, C. N. (2012). Interstitial stem cells in Hydra: multipotency and decision-making. *Int J Dev Biol*, *56*(6-8), 489-497. https://doi.org/10.1387/ijdb.113476cd

Denker, E., Manuel, M., Leclère, L., Le Guyader, H., & Rabet, N. (2008). Ordered progression of nematogenesis from stem cells through differentiation stages in the tentacle bulb of Clytia hemisphaerica (Hydrozoa, Cnidaria). *Developmental Biology*, *315*(1), 99-113. https://doi.org/https://doi.org/10.1016/j.ydbio.2007.12.023

DuBuc, T. Q., Traylor-Knowles, N., & Martindale, M. Q. (2014). Initiating a regenerative response; cellular and molecular features of wound healing in the cnidarian Nematostella vectensis. *BMC Biology*, *12*(1), 24. https://doi.org/10.1186/1741-7007-12-24

Finnerty, J. R. (2001). Cnidarians Reveal Intermediate Stages in the Evolution of Hox Clusters and Axial Complexity1. *American Zoologist*, *41*(3), 608-620. https://doi.org/10.1093/icb/41.3.608

Florio, M., & Huttner, W. B. (2014). Neural progenitors, neurogenesis and the evolution of the neocortex. *Development*, *141*(11), 2182-2194. https://doi.org/10.1242/dev.090571

Freeman, S. C., Malik, A., & Basit, H. (2020). *Physiology, Exocrine Gland*. StatPearls Publishing, Treasure Island (FL). http://europepmc.org/abstract/MED/31194462

Fritz, A. E., Ikmi, A., Seidel, C., Paulson, A., & Gibson, M. C. (2013). Mechanisms of tentacle morphogenesis in the sea anemone Nematostella vectensis. *Development*, *140*(10), 2212-2223. https://doi.org/10.1242/dev.088260

Fritzenwanker, J. H., Genikhovich, G., Kraus, Y., & Technau, U. (2007). Early development and axis specification in the sea anemone Nematostella vectensis. *Developmental Biology*, *310*(2), 264-279. https://doi.org/https://doi.org/10.1016/j.ydbio.2007.07.029

Fritzenwanker, J. H., & Technau, U. (2002). Induction of gametogenesis in the basal cnidarian Nematostella vectensis (Anthozoa). *Development Genes and Evolution*, *212*(2), 99-103. https://doi.org/10.1007/s00427-002-0214-7

Fuller, Z. L., Mocellin, V. J. L., Morris, L. A., Cantin, N., Shepherd, J., Sarre, L., Peng, J., Liao, Y., Pickrell, J., Andolfatto, P., Matz, M., Bay, L. K., & Przeworski, M. (2020). Population genetics of the coral Acropora millepora: Toward genomic prediction of bleaching. *Science*, *369*(6501). https://doi.org/10.1126/science.aba4674

Gahan, J. M., Bradshaw, B., Flici, H., & Frank, U. (2016). The interstitial stem cells in Hydractinia and their role in regeneration. *Current Opinion in Genetics & Development*, *40*, 65-73. https://doi.org/https://doi.org/10.1016/j.gde.2016.06.006

Gahan, J. M., Kouzel, I. U., & Rentzsch, F. (2020). Histone demethylase Lsd1 is required for the differentiation of neural cells in the cnidarian <em>Nematostella vectensis</em&gt. *bioRxiv*, 2020.2009.2007.285577. https://doi.org/10.1101/2020.09.07.285577

Galliot, B., Quiquand, M., Ghila, L., de Rosa, R., Miljkovic-Licina, M., & Chera, S. (2009). Origins of neurogenesis, a cnidarian view. *Developmental Biology*, *332*(1), 2-24. https://doi.org/https://doi.org/10.1016/j.ydbio.2009.05.563

Gauchat, D., Mazet, F., Berney, C., Schummer, M., Kreger, S., Pawlowski, J., & Galliot, B. (2000). Evolution of Antp-class genes and differential expression of Hydra Hox/paraHox genes in anterior patterning. *Proceedings of the National Academy of Sciences*, *97*(9), 4493. https://doi.org/10.1073/pnas.97.9.4493

Gont, L. K., Fainsod, A., Kim, S.-H., & De Robertis, E. M. (1996). Overexpression of the Homeobox Gene Xnot-2 Leads to Notochord Formation inXenopus. *Developmental Biology*, *174*(1), 174-178. https://doi.org/https://doi.org/10.1006/dbio.1996.0061

Götz, M., & Huttner, W. B. (2005). The cell biology of neurogenesis. *Nature Reviews Molecular Cell Biology*, *6*(10), 777-788. https://doi.org/10.1038/nrm1739

Graham, V., Khudyakov, J., Ellis, P., & Pevny, L. (2003). SOX2 Functions to Maintain Neural Progenitor Identity. *Neuron*, *39*(5), 749-765. https://doi.org/https://doi.org/10.1016/S0896-6273(03)00497-5

Halpern, M. E., Thisse, C., Ho, R. K., Thisse, B., Riggleman, B., Trevarrow, B., Weinberg, E. S., Postlethwait, J. H., & Kimmel, C. B. (1995). Cell-autonomous shift from axial to paraxial mesodermal development in zebrafish floating head mutants. *Development*, *121*(12), 4257-4264. https://doi.org/10.1242/dev.121.12.4257

Hand, C., & Uhlinger, K. R. (1992). The Culture, Sexual and Asexual Reproduction, and Growth of the Sea Anemone Nematostella vectensis. *The Biological Bulletin*, *182*(2), 169-176. https://doi.org/10.2307/1542110

Hardwick, L. J. A., Ali, F. R., Azzarelli, R., & Philpott, A. (2015). Cell cycle regulation of proliferation versus differentiation in the central nervous system. *Cell and Tissue Research*, *359*(1), 187-200. https://doi.org/10.1007/s00441-014-1895-8

Hartenstein, V., Takashima, S., Hartenstein, P., Asanad, S., & Asanad, K. (2017). bHLH proneural genes as cell fate determinants of entero-endocrine cells, an evolutionarily conserved lineage sharing a common root with sensory neurons. *Developmental Biology*, *431*(1), 36-47. https://doi.org/https://doi.org/10.1016/j.ydbio.2017.07.013

Hartenstein, V., & Wodarz, A. (2013). Initial neurogenesis in Drosophila [https://doi.org/10.1002/wdev.111]. *WIREs Developmental Biology*, *2*(5), 701-721. https://doi.org/https://doi.org/10.1002/wdev.111

He, S., Del Viso, F., Chen, C.-Y., Ikmi, A., Kroesen, A. E., & Gibson, M. C. (2018). An axial Hox code controls tissue segmentation and body patterning in Nematostella vectensis. *Science*, *361*(6409), 1377-1380.

Hedges, S. B. (2002). The origin and evolution of model organisms. *Nature Reviews Genetics*, *3*(11), 838-849. https://doi.org/10.1038/nrg929

Hejnol, A., Obst, M., Stamatakis, A., Ott, M., Rouse, G. W., Edgecombe, G. D., Martinez, P., Baguñà, J., Bailly, X., Jondelius, U., Wiens, M., Müller, W. E. G., Seaver, E., Wheeler, W. C., Martindale, M. Q., Giribet, G., & Dunn, C. W. (2009). Assessing the root of bilaterian animals with scalable phylogenomic methods. *Proceedings of the Royal Society B: Biological Sciences*, *276*(1677), 4261-4270. https://doi.org/doi:10.1098/rspb.2009.0896

Holland, P. W. H. (2013). Evolution of homeobox genes [https://doi.org/10.1002/wdev.78]. *WIREs Developmental Biology*, *2*(1), 31-45. https://doi.org/https://doi.org/10.1002/wdev.78

Ikezawa, T., Goso, Y., Ichikawa, T., Hayashida, H., Kurihara, M., Okayasu, I., Saigenji, K., & Ishihara, K. (2004). Appearance of specific mucins recognized by monoclonal antibodies in rat gastric

mucosa healing from HCl-induced gastric mucosal damage. *Journal of gastroenterology*, *39*(2), 113-119.

Ikmi, A., McKinney, S. A., Delventhal, K. M., & Gibson, M. C. (2014). TALEN and CRISPR/Cas9-mediated genome editing in the early-branching metazoan Nematostella vectensis. *Nature Communications*, *5*(1), 5486. https://doi.org/10.1038/ncomms6486

Ikmi, A., Steenbergen, P. J., Anzo, M., McMullen, M. R., Stokkermans, A., Ellington, L. R., & Gibson, M. C. (2020). Feeding-dependent tentacle development in the sea anemone Nematostella vectensis. *Nature Communications*, *11*(1), 4399. https://doi.org/10.1038/s41467-020-18133-0

Jékely, G. (2021). The chemical brain hypothesis for the origin of nervous systems. *Philosophical transactions of the Royal Society of London. Series B, Biological sciences*, *376*(1821), 20190761-20190761. https://doi.org/10.1098/rstb.2019.0761

Karabulut, A., He, S., Chen, C. Y., McKinney, S. A., & Gibson, M. C. (2019). Electroporation of short hairpin RNAs for rapid and efficient gene knockdown in the starlet sea anemone, Nematostella vectensis. *Dev Biol*, *448*(1), 7-15. https://doi.org/10.1016/j.ydbio.2019.01.005

Kelava, I., Rentzsch, F., & Technau, U. (2015). Evolution of eumetazoan nervous systems: insights from cnidarians. *Philosophical transactions of the Royal Society of London. Series B, Biological sciences*, *370*(1684), 20150065. https://doi.org/10.1098/rstb.2015.0065

Kristan, W. B. (2016). Early evolution of neurons. *Current Biology*, *26*(20), R949-R954. https://doi.org/https://doi.org/10.1016/j.cub.2016.05.030

Layden, M. J., Boekhout, M., & Martindale, M. Q. (2012). Nematostella vectensis achaete-scute homolog NvashA regulates embryonic ectodermal neurogenesis and represents an ancient component of the metazoan neural specification pathway. *Development*, *139*(5), 1013-1022. https://doi.org/10.1242/dev.073221

Layden, M. J., & Martindale, M. Q. (2014). Non-canonical Notch signaling represents an ancestral mechanism to regulate neural differentiation. *Evodevo*, *5*(1), 30. https://doi.org/10.1186/2041-9139-5-30

Layden, M. J., Rentzsch, F., & Röttinger, E. (2016). The rise of the starlet sea anemone Nematostella vectensis as a model system to investigate development and regeneration. *WIREs Developmental Biology*, *5*(4), 408-428. https://doi.org/https://doi.org/10.1002/wdev.222

Layden, M. J., Röttinger, E., Wolenski, F. S., Gilmore, T. D., & Martindale, M. Q. (2013). Microinjection of mRNA or morpholinos for reverse genetic analysis in the starlet sea anemone, Nematostella vectensis. *Nat Protoc*, *8*(5), 924-934. https://doi.org/10.1038/nprot.2013.009

Lee, P. N., Kumburegama, S., Marlow, H. Q., Martindale, M. Q., & Wikramanayake, A. H. (2007). Asymmetric developmental potential along the animal–vegetal axis in the anthozoan cnidarian, Nematostella vectensis, is mediated by Dishevelled. *Developmental Biology*, *310*(1), 169-186. https://doi.org/https://doi.org/10.1016/j.ydbio.2007.05.040

Lenhoff, H. M., & Lenhoff, S. G. (1989). Challenge to the specialist: Abraham Trembley's approach to research on the organism - 1744 and today. *American Zoologist*, *29*(3), 1105-1117.

Levitan, S., Sher, N., Brekhman, V., Ziv, T., Lubzens, E., & Lotan, T. (2015). The making of an embryo in a basal metazoan: Proteomic analysis in the sea anemone Nematostella vectensis [https://doi.org/10.1002/pmic.201500255]. *PROTEOMICS*, *15*(23-24), 4096-4104. https://doi.org/https://doi.org/10.1002/pmic.201500255

Magie, C. R., Pang, K., & Martindale, M. Q. (2005). Genomic inventory and expression of Sox and Fox genes in the cnidarian Nematostella vectensis. *Dev Genes Evol*, *215*(12), 618-630. https://doi.org/10.1007/s00427-005-0022-y

Mark, M., Rijli, F. M., & Chambon, P. (1997). Homeobox Genes in Embryogenesis and Pathogenesis. *Pediatric Research*, *42*(4), 421-429. https://doi.org/10.1203/00006450-199710000-00001

Marlow, H., Roettinger, E., Boekhout, M., & Martindale, M. Q. (2012). Functional roles of Notch signaling in the cnidarian Nematostella vectensis. *Developmental Biology*, *362*(2), 295-308.

Marlow, H. Q., Srivastava, M., Matus, D. Q., Rokhsar, D., & Martindale, M. Q. (2009). Anatomy and development of the nervous system of Nematostella vectensis, an anthozoan cnidarian [https://doi.org/10.1002/dneu.20698]. *Developmental Neurobiology*, *69*(4), 235-254. https://doi.org/https://doi.org/10.1002/dneu.20698

Martindale, M. Q., Pang, K., & Finnerty, J. R. (2004). Investigating the origins of triploblasty: `mesodermal' gene expression in a diploblastic animal, the sea anemone Nematostella vectensis(phylum, Cnidaria; class, Anthozoa). *Development*, *131*(10), 2463-2474. https://doi.org/10.1242/dev.01119

Moroz, L. L. (2009). On the Independent Origins of Complex Brains and Neurons. *Brain, Behavior and Evolution*, *74*(3), 177-190. https://doi.org/10.1159/000258665

Nakanishi, N., Renfer, E., Technau, U., & Rentzsch, F. (2012). Nervous systems of the sea anemone Nematostella vectensis are generated by ectoderm and endoderm and shaped by distinct mechanisms. *Development*, *139*(2), 347-357. https://doi.org/10.1242/dev.071902

Negre, B., & Ruiz, A. (2007). HOM-C evolution in Drosophila: is there a need for Hox gene clustering? *Trends in Genetics*, *23*(2), 55-59. https://doi.org/https://doi.org/10.1016/j.tig.2006.12.001

Putnam, N. H., Srivastava, M., Hellsten, U., Dirks, B., Chapman, J., Salamov, A., Terry, A., Shapiro, H., Lindquist, E., Kapitonov, V. V., Jurka, J., Genikhovich, G., Grigoriev, I. V., Lucas, S. M., Steele, R. E., Finnerty, J. R., Technau, U., Martindale, M. Q., & Rokhsar, D. S. (2007). Sea Anemone Genome Reveals Ancestral Eumetazoan Gene Repertoire and Genomic Organization. *Science*, *317*(5834), 86. https://doi.org/10.1126/science.1139158

Renfer, E., Amon-Hassenzahl, A., Steinmetz, P. R., & Technau, U. (2010). A muscle-specific transgenic reporter line of the sea anemone, Nematostella vectensis. *Proc Natl Acad Sci U S A*, *107*(1), 104-108. https://doi.org/10.1073/pnas.0909148107

Rentzsch, F., Layden, M., & Manuel, M. (2017). The cellular and molecular basis of cnidarian neurogenesis [https://doi.org/10.1002/wdev.257]. *WIREs Developmental Biology*, *6*(1), e257. https://doi.org/https://doi.org/10.1002/wdev.257

Rentzsch, F., Renfer, E., & Technau, U. (2020). Generating Transgenic Reporter Lines for Studying Nervous System Development in the Cnidarian Nematostella vectensis. *Methods Mol Biol*, *2047*, 45-57. https://doi.org/10.1007/978-1-4939-9732-9_3

Rentzsch, F., & Technau, U. (2016). Genomics and development of Nematostella vectensis and other anthozoans. *Current Opinion in Genetics & Development*, *39*, 63-70. https://doi.org/https://doi.org/10.1016/j.gde.2016.05.024

Richards, G. S., & Rentzsch, F. (2014). Transgenic analysis of a SoxB gene reveals neural progenitor cells in the cnidarian Nematostella vectensis. *Development*, *141*(24), 4681-4689. https://doi.org/10.1242/dev.112029

Richards, G. S., & Rentzsch, F. (2015). Regulation of Nematostella neural progenitors by SoxB, Notch and bHLH genes. *Development*, *142*(19), 3332-3342. https://doi.org/10.1242/dev.123745

Russell, J. J., Theriot, J. A., Sood, P., Marshall, W. F., Landweber, L. F., Fritz-Laylin, L., Polka, J. K., Oliferenko, S., Gerbich, T., Gladfelter, A., Umen, J., Bezanilla, M., Lancaster, M. A., He, S., Gibson, M. C., Goldstein, B., Tanaka, E. M., Hu, C. K., & Brunet, A. (2017). Non-model model organisms. *BMC Biol*, *15*(1), 55. https://doi.org/10.1186/s12915-017-0391-5

Schindelin, J., Arganda-Carreras, I., Frise, E., Kaynig, V., Longair, M., Pietzsch, T., Preibisch, S., Rueden, C., Saalfeld, S., Schmid, B., Tinevez, J.-Y., White, D. J., Hartenstein, V., Eliceiri, K., Tomancak, P., & Cardona, A. (2012). Fiji: an open-source platform for biological-image analysis. *Nature Methods*, *9*(7), 676-682. https://doi.org/10.1038/nmeth.2019

Schmidt-Rhaesa, A., Harzsch, S., & Purschke, G. (2015). *Structure and evolution of invertebrate nervous systems*. Oxford University Press.

Sebé-Pedrós, A., Saudemont, B., Chomsky, E., Plessier, F., Mailhé, M.-P., Renno, J., Loe-Mie, Y., Lifshitz, A., Mukamel, Z., Schmutz, S., Novault, S., Steinmetz, P. R. H., Spitz, F., Tanay, A., & Marlow, H. (2018). Cnidarian Cell Type Diversity and Regulation Revealed by Whole-Organism Single-Cell RNA-Seq. *Cell*, *173*(6), 1520-1534.e1520. https://doi.org/https://doi.org/10.1016/j.cell.2018.05.019

Siebert, S., Anton-Erxleben, F., & Bosch, T. C. G. (2008). Cell type complexity in the basal metazoan Hydra is maintained by both stem cell based mechanisms and transdifferentiation. *Developmental Biology*, *313*(1), 13-24. https://doi.org/https://doi.org/10.1016/j.ydbio.2007.09.007

Siebert, S., Farrell, J. A., Cazet, J. F., Abeykoon, Y., Primack, A. S., Schnitzler, C. E., & Juliano, C. E. (2019). Stem cell differentiation trajectories in Hydra resolved at single-cell resolution. *Science (New York, N.Y.)*, *365*(6451), eaav9314. https://doi.org/10.1126/science.aav9314

Smith, Carolyn L., Varoqueaux, F., Kittelmann, M., Azzam, Rita N., Cooper, B., Winters, Christine A., Eitel, M., Fasshauer, D., & Reese, Thomas S. (2014). Novel Cell Types, Neurosecretory Cells, and Body Plan of the Early-Diverging Metazoan Trichoplax adhaerens. *Current Biology*, *24*(14), 1565-1572. https://doi.org/https://doi.org/10.1016/j.cub.2014.05.046

Stein, S., & Kessel, M. (1995). A homeobox gene involved in node, notochord and neural plate formation of chick embryos. *Mechanisms of Development*, *49*(1), 37-48. https://doi.org/https://doi.org/10.1016/0925-4773(94)00300-C

Steinmetz, P. R. H. (2019). A non-bilaterian perspective on the development and evolution of animal digestive systems. *Cell and Tissue Research*, *377*(3), 321-339. https://doi.org/10.1007/s00441-019-03075-x

Steinmetz, P. R. H., Aman, A., Kraus, J. E. M., & Technau, U. (2017). Gut-like ectodermal tissue in a sea anemone challenges germ layer homology. *Nature Ecology & Evolution*, *1*(10), 1535-1542. https://doi.org/10.1038/s41559-017-0285-5

Talbot, W. S., Trevarrow, B., Halpern, M. E., Melby, A. E., Farr, G., Postlethwait, J. H., Jowett, T., Kimmel, C. B., & Kimelman, D. (1995). A homeobox gene essential for zebrafish notochord development. *Nature*, *378*(6553), 150-157. https://doi.org/10.1038/378150a0

Taverna, E., Götz, M., & Huttner, W. B. (2014). The Cell Biology of Neurogenesis: Toward an Understanding of the Development and Evolution of the Neocortex. *Annual Review of Cell and Developmental Biology*, *30*(1), 465-502. https://doi.org/10.1146/annurev-cellbio-101011-155801

Technau, U., & Steele, R. E. (2012). Evolutionary crossroads in developmental biology: Cnidaria (vol 138, pg 1447, 2011). *Development*, *139*(23), 4491-4491. https://doi.org/10.1242/dev.090472

Tournière, O., Busengdal, H., Gahan, J. M., & Rentzsch, F. (2021). Insm1-expressing neurons and secretory cells develop from a common pool of progenitors in the sea anemone Nematostella vectensis. *bioRxiv*, 2021.2004.2009.439178. https://doi.org/10.1101/2021.04.09.439178

Tournière, O., Dolan, D., Richards, G. S., Sunagar, K., Columbus-Shenkar, Y. Y., Moran, Y., & Rentzsch, F. (2020). NvPOU4/Brain3 Functions as a Terminal Selector Gene in the Nervous System of the Cnidarian Nematostella vectensis. *Cell Reports*, *30*(13), 4473-4489.e4475. https://doi.org/https://doi.org/10.1016/j.celrep.2020.03.031

Trembley, A. (1744). *Mémoires, pour servir à l'histoire d'un genre de polypes d'eau douce, à bras en forme de cornes* (Vol. 1). Chez Jean & Herman Verbeek.

Truman, J. W., & Bate, M. (1988). Spatial and temporal patterns of neurogenesis in the central nervous system of Drosophila melanogaster. *Developmental Biology*, *125*(1), 145-157. https://doi.org/https://doi.org/10.1016/0012-1606(88)90067-X

von Dassow, G., Schmidt, J. E., & Kimelman, D. (1993). Induction of the Xenopus organizer: expression and regulation of Xnot, a novel FGF and activin-regulated homeo box gene. *Genes Dev*, *7*(3), 355-366. https://doi.org/10.1101/gad.7.3.355

Watanabe, H., Kuhn, A., Fushiki, M., Agata, K., Özbek, S., Fujisawa, T., & Holstein, T. W. (2014). Sequential actions of β-catenin and Bmp pattern the oral nerve net in Nematostella vectensis. *Nature Communications*, *5*(1), 5536. https://doi.org/10.1038/ncomms6536

Williams, R. B. (1975). A redescription of the brackish-water sea anemone Nematostella vectensis Stephenson, with an appraisal of congeneric species. *Journal of Natural History*, *9*(1), 51-64. https://doi.org/10.1080/00222937500770051

Williams, R. B. (1979). Studies on the Nematosomes of Nematostella-Vectensis Stephenson (Coelenterata Actiniaria). *Journal of Natural History*, *13*(1), 69-80. https://doi.org/Doi 10.1080/00222937900770061

Wolenski, F. S., Bradham, C. A., Finnerty, J. R., & Gilmore, T. D. (2013). NF-κB is required for cnidocyte development in the sea anemone Nematostella vectensis. *Developmental Biology*, *373*(1), 205-215. https://doi.org/https://doi.org/10.1016/j.ydbio.2012.10.004

Yasuo, H., & Lemaire, P. (2001). Role of Goosecoid, Xnot and Wnt antagonists in the maintenance of the notochord genetic programme in Xenopus gastrulae. *Development*, *128*(19), 3783-3793. https://www.ncbi.nlm.nih.gov/pubmed/11585804

Zenkert, C., Takahashi, T., Diesner, M. O., & Ozbek, S. (2011). Morphological and molecular analysis of the Nematostella vectensis cnidom. *PLoS One*, *6*(7), e22725. https://doi.org/10.1371/journal.pone.0022725

Zhao, G., & Skeath, J. B. (2002). The Sox-domain containing gene Dichaete/fish-hook acts in concert with vnd and ind to regulate cell fate in the Drosophila neuroectoderm. *Development*, *129*(5), 1165-1174. https://doi.org/10.1242/dev.129.5.1165

Zhong, W., & Chia, W. (2008). Neurogenesis and asymmetric cell division. *Current Opinion in Neurobiology*, *18*(1), 4-11. https://doi.org/https://doi.org/10.1016/j.conb.2008.05.002